Marine Pollution Bulletin 189 (2023) 114765

Contents lists available at ScienceDirect

Marine Pollution Bulletin

journal homepage: www.elsevier.com/locate/marpolbul

Contamination of planktonic food webs in the Mediterranean Sea: Setting the frame for the MERITE-HIPPOCAMPE oceanographic cruise (spring 2019)☆

Marc Tedetti [a,*], Jacek Tronczynski [b], François Carlotti [a], Marc Pagano [a], Sana Ben Ismail [c], Cherif Sammari [c], Malika Bel Hassen [c], Karine Desboeufs [d], Charlotte Poindron [d], Sandrine Chifflet [a], Amel Bellaaj Zouari [c], Moufida Abdennadher [c], Sirine Amri [c], Daniela Bănaru [a], Lotfi Ben Abdallah [c], Nagib Bhairy [a], Ismail Boudriga [c], Aude Bourin [e], Christophe Brach-Papa [f], Nicolas Briant [b], Léa Cabrol [a], Cristele Chevalier [a], Lassaad Chouba [c], Sylvain Coudray [f], Mohamed Nejib Daly Yahia [g], Thibault de Garidel-Thoron [h], Aurélie Dufour [a], Jean-Claude Dutay [i], Boris Espinasse [j], Pamela Fierro-González [a], Michel Fornier [a], Nicole Garcia [a], Franck Giner [k], Catherine Guigue [a], Loïc Guilloux [a], Asma Hamza [c], Lars-Eric Heimbürger-Boavida [a], Stéphanie Jacquet [a], Joel Knoery [b], Rim Lajnef [c], Nouha Makhlouf Belkahia [l,m], Deny Malengros [a], Pauline L. Martinot [a], Anthony Bosse [a], Jean-Charles Mazur [h], Marouan Meddeb [m,n], Benjamin Misson [o], Olivier Pringault [a], Marianne Quéméneur [a], Olivier Radakovitch [h,k], Patrick Raimbault [a], Christophe Ravel [f], Vincent Rossi [a], Chaimaa Rwawi [a], Asma Sakka Hlaili [m,n], Javier Angel Tesán-Onrubia [o], Bastien Thomas [b], Melilotus Thyssen [a], Noureddine Zaaboub [c], Cédric Garnier [o]

[a] Aix Marseille Univ., Université de Toulon, CNRS, IRD, MIO, Marseille, France
[b] Ifremer, CCEM Contamination Chimique des Ecosystèmes Marins, F-44311 Nantes, France
[c] Institut National des Sciences et Technologies de la Mer (INSTM), 28, rue 2 mars 1934, Salammbô 2025, Tunisia
[d] Université Paris Cité et Université Paris-Est Creteil, CNRS, LISA, F-75013 Paris, France
[e] IMT Nord Europe, Institut Mines-Télécom, Univ. Lille, Centre for Energy and Environment, F-59000 Lille, France
[f] Ifremer, Unité Littoral, Laboratoire Environnement Ressources Provence Azur Corse, Zone portuaire de Brégaillon, CS 20330, 83507 La Seyne-sur-Mer Cedex, France
[g] Environmental Sciences Program, Department of Biological and Environmental Sciences, College of Arts and Sciences, Qatar University, PO Box 2713, Doha, Qatar
[h] Aix Marseille Univ., CNRS, IRD, Collège de France, INRAE, CEREGE, 13545 Aix-en-Provence Cedex 4, France
[i] Laboratoire des Sciences du Climat et de l'Environnement LSCE/IPSL, CEA-CNRS-UVSQ, Université Paris-Saclay, 91191 Gif-sur-Yvette, France
[j] Department of Arctic and Marine Biology, UiT The Arctic University of Norway, Tromsø, Norway
[k] Institut de Radioprotection et de Sûreté Nucléaire (IRSN), PSE-SRTE-LRTA, Cadarache, France
[l] Université de Carthage, Faculté des Sciences de Bizerte, Bizerte, Tunisia
[m] Université de Tunis El Manar, Faculté des Sciences de Tunis, Laboratoire des Sciences de l'Environnement, Biologie et Physiologie des Organismes Aquatiques LR18ES41, Tunis, Tunisia
[n] Université de Carthage, Faculté des Sciences de Bizerte, Laboratoire de Biologie Végétale et Phytoplanctonologie, Bizerte, Tunisia
[o] Université de Toulon, Aix Marseille Univ., CNRS, IRD, MIO, Toulon, France

ARTICLE INFO

Keywords:
Contaminants
Plankton
Mediterranean Sea

ABSTRACT

This paper looks at experiential feedback and the technical and scientific challenges tied to the MERITE-HIPPOCAMPE cruise that took place in the Mediterranean Sea in spring 2019. This cruise proposes an innovative approach to investigate the accumulation and transfer of inorganic and organic contaminants within the planktonic food webs. We present detailed information on how the cruise worked, including 1) the cruise track

☆ For submission to Marine Pollution Bulletin – Special issue "Plankton and Contaminants in the Mediterranean Sea: Biological pump and interactions from regional to global approaches"

* Corresponding author.
E-mail address: marc.tedetti@mio.osupytheas.fr (M. Tedetti).

https://doi.org/10.1016/j.marpolbul.2023.114765
Received 28 July 2022; Received in revised form 9 February 2023; Accepted 19 February 2023
Available online 8 March 2023

Size fractions
Bioaccumulation
Atmospheric deposition

and sampling stations, 2) the overall strategy, based mainly on the collection of plankton, suspended particles and water at the deep chlorophyll maximum, and the separation of these particles and planktonic organisms into various size fractions, as well as the collection of atmospheric deposition, 3) the operations performed and material used at each station, and 4) the sequence of operations and main parameters analysed. The paper also provides the main environmental conditions that were prevailing during the campaign. Lastly, we present the types of articles produced based on work completed by the cruise that are part of this special issue.

1. Introduction

Plankton is recognised as a key gateway of inorganic and organic contaminants into the marine food web (Berrojalbiz et al., 2011; Tao et al., 2018; Chouvelon et al., 2019; Li et al., 2021). Phytoplankton exposure to contaminants is mainly via water. Phytoplankton cells have a high surface area-to-volume ratio and thus large areas for exchanges, and consequently display high capacities for adsorbing and absorbing and thus bioconcentrating dissolved contaminants (Martin and Knauer, 1973; Fan and Reinfelder, 2003; Heimbürger et al., 2010; Lee and Fisher, 2016; Chouvelon et al., 2019). Contaminant bioconcentration in phytoplankton, thought to be governed mainly by partition equilibrium processes between the cells and the surrounding water (Frouin et al., 2013) even though cell growth conditions may prevent contaminants from reaching thermodynamic equilibrium (Swackhamer and Skoglund, 1993), tends to increase with decreasing size of algal cells (Fan and Reinfelder, 2003).

Bioaccumulation processes in zooplankton are highly complex due to 1) entry of contaminants by both the water aqueous phase (bioconcentration) and diet, 2) trophic interactions and/or transfers between phytoplankton and herbivorous, carnivorous and omnivorous zooplankton, and 3) the contaminant elimination processes used by these organisms, including metabolization, excretion and passive release (Tiano et al., 2014; Alekseenko et al., 2018; Tao et al., 2018; Thomas et al., 2018; Li et al., 2020). The fact that all these processes can act simultaneously in the same or opposite directions makes it difficult to understand the variability of contaminant concentrations within the planktonic food web, which may ultimately display biomagnification (increasing contaminant concentrations with trophic level), bioreduction (decreasing contaminant concentrations with trophic level) or no clear pattern (Nizzetto et al., 2012; Tiano et al., 2014; Strady et al., 2015; Tao et al., 2017a, 2017b; Alekseenko et al., 2018; Chouvelon et al., 2019; Tang et al., 2020; Castro-Jiménez et al., 2021; Li et al., 2021).

One important biogeochemical implication of contaminant uptake by plankton is the role as a "biological pump" for contaminant sequestration (Dachs et al., 2002; Galbán-Malagón et al., 2012; Duran and Cravo-Laureau, 2016; González-Gaya et al., 2019; Tang et al., 2020). Contaminants bioconcentrated/bioaccumulated within planktonic organisms subsequently get transferred to higher trophic levels or to deep waters and sediment through sinking particles. During phytoplankton blooms, contaminant uptake by plankton depletes the contaminant loads in the dissolved phase of the water column and increases contaminant air-water fluxes, sinking particle fluxes and sequestration in sediments (Berrojalbiz et al., 2011; Nizzetto et al., 2012; Everaert et al., 2015; Morales et al., 2015; Casal et al., 2017; Ding et al., 2021).

The phosphorus-limited Mediterranean Sea is globally classified as an oligotrophic marine area (D'Ortenzio and d'Alcalà, 2009; The Mermex Group, 2011; Marañón et al., 2021) dominated by small phytoplankton (i.e., pico- and nano-sized fractions) (Uitz et al., 2006; Hunt et al., 2017; Mayot et al., 2017; Leblanc et al., 2018; Salhi et al., 2018; Ramírez-Romero et al., 2020), even though the occurrence of regional phytoplankton blooms (bloom bioregions, ecoregions; D'Ortenzio and d'Alcalà, 2009; Berline et al., 2014; Reygondeau et al., 2017; Ayata et al., 2018) leads to periods of coexistence of numerous microalgal groups (Siokou-Frangou et al., 2010; El Hourany et al., 2019).

Another feature of the Mediterranean Sea is its high exposure to chemical contamination (Hinrichsen, 1990; The Mermex Group, 2011; UNEP/MAP, 2012). Indeed, the intense human activities in its 23 bordering countries induce significant inputs of various chemical contaminants, while its semi-closed geography limits possibilities for diluting them. Contaminants are brought to the Mediterranean mainly by major and smaller river systems (Elbaz-Poulichet et al., 2001; Radakovitch et al., 2008; Sicre et al., 2008; Guigue et al., 2014; Köck-Schulmeyer et al., 2021) but also via effluents, runoffs, groundwater, and maritime activities (Tedetti et al., 2010; Oursel et al., 2013; Tornero and Hanke, 2016; Fourati et al., 2018; Jacquet et al., 2021; Llamas-Dios et al., 2021) as well as atmospheric deposition (Lipiatou and Albaigés, 1994; Heimbürger et al., 2011; Castro-Jiménez et al., 2017; Barhoumi et al., 2018; Desboeufs et al., 2022). Studies have demonstrated that atmospheric deposition is the major source of contaminants in remote/open sea areas (Dachs and Méjanelle, 2010; González-Gaya et al., 2019; Jiskra et al., 2021; Cossa et al., 2022).

An interesting feature of the bioaccumulation of contaminants in the Mediterranean Sea is that the recorded contamination levels are significantly higher in its predatory species (crustaceans, sharks, teleost fish) than in congeneric species of the Atlantic Ocean (Cossa and Coquery, 2005; Bodiguel et al., 2009; Chouvelon et al., 2018). This difference may be related (but not solely) to the enhanced ability of the Mediterranean planktonic food webs to bioaccumulate certain contaminants, such as mercury (Hg) (Cossa and Coquery, 2005; Harmelin-Vivien et al., 2009; Chouvelon et al., 2018, 2019; Cossa et al., 2022), which further underscores the potential key role of the planktonic compartment in the transfer and accumulation of contaminants in the Mediterranean Sea. Furthermore, contaminant-plankton interactions in the Mediterranean Sea are expected to evolve in the coming years, as it has been identified as a hotspot for climate change due to its high reactivity to external forcing, particularly variations in water, energy and matter fluxes that will affect its circulation, biogeochemical fluxes and ecosystem functioning (Lejeusne et al., 2010; The Mermex Group, 2011; Ser-Giacomi et al., 2020).

However, there are still key gaps in our understanding around the actual ability of plankton to accumulate and transfer contaminants (i.e., the role of plankton as a biological pump of contaminants), especially its small size fractions, i.e., pico- and nano-plankton. This lack of knowledge partly comes from methodological difficulties in: 1) collecting and separating plankton into its various size fractions from pico- to macroplankton, separating bacterio-, phyto- from zoo-plankton, and separating non-living suspended particulate matter from plankton, 2) obtaining sufficient material in each of these fractions to perform trace-level chemical analyses, and 3) clearly identifying the trophic relationships between planktonic size fractions in the presence of detritus (particularly in smaller size fractions) and mixing of different trophic levels within each size fraction.

In this context, the MERITE-HIPPOCAMPE cruise aimed to evaluate the accumulation and transfer of a hugely diverse range of inorganic and organic contaminants at the atmosphere-water-plankton interfaces and within the planktonic food webs, i.e., phyto-, zoo- and bacterioplankton, along a North-South transect in the Mediterranean Sea. This ultimately to quantify the role of Mediterranean plankton as a biological pump of contaminants, focusing on contaminant transfers into the planktonic food webs. The main collection area for plankton, suspended particles and water is the deep chlorophyll maximum (DCM), which may be considered as the layer with the highest biomasses of plankton,

mainly phytoplankton, but also zooplankton. The plankton size fractions investigated include pico- (0.2–2 μm), nano- (2–20 μm), micro- (20–200 μm) and meso-plankton (200–2000 μm). The contaminants examined are trace metals, organometals and metalloids (As, Cd, Cr, Cu, Fe, Hg, MeHg, Mn, Ni, Pb, Sb, Zn…), organic contaminants (PAHs, PCBs, PBDEs, PFASs), radionuclides (^{137}Cs), and microplastics. The specific objectives of the cruise are: 1) to determine the contaminant concentration levels in various planktonic compartments (phyto-, zoo- and bacterio-plankton), suspended particles and water (dissolved phase), as well as atmosphere and, 2) to assess the role of dry/wet atmospheric deposition as a source of contaminants for marine waters, especially in offshore areas, 3) to gauge how contaminant accumulations and transfers are influenced by plankton in terms of size and community structures, trophic interactions and biochemical content, and 4) to establish the link between habitat characteristics and concentration levels of contaminants in plankton. The questions addressed by the MERITE-HIPPOCAMPE cruise are summarised in Fig. 1. In this paper, we first present the implementation of the cruise project in terms of strategy, study stations, material used, operations performed, sequence of operations, and main parameters analysed. We then work up from a joint dataset to provide the main meteorological, hydrological, and biogeochemical conditions prevailing during the cruise. Lastly, we introduce the types of articles produced through the MERITE-HIPPOCAMPE cruise that are part of this special issue.

2. Implementation of the cruise

2.1. Research strategy

The overall research strategy for our oceanographic cruise was as follows:

1) Investigate areas of contrasted ecological characteristics in the north and south of the Mediterranean Sea. The selected period was the spring bloom, crossing primary production and bloom areas as defined by D'Ortenzio and d'Alcalà (2009) as well as various fishing zones, urbanised bays, and consensus regions as defined by Ayata et al. (2018) (Figs. 2a, b; S1).
2) Characterise the water column in these sampling sites in terms of physical and biogeochemical properties through in situ physical and optical measurements, and determine the DCM.

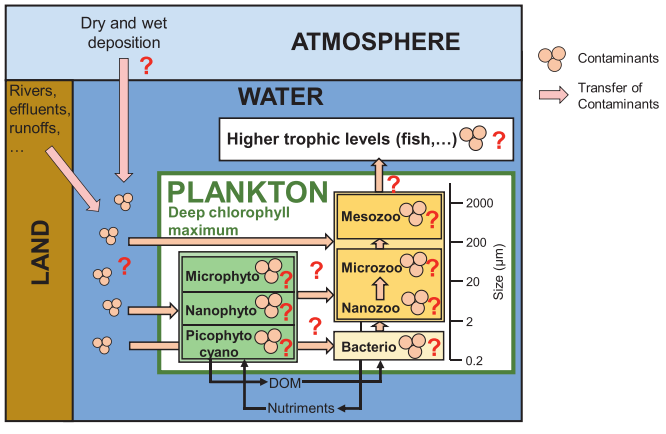

Fig. 1. Conceptual scheme and questions addressed by the MERITE-HIPPOCAMPE cruise to identify the role of Mediterranean plankton as biological pump of contaminants. It considers the accumulation and transfer of metallic/metalloid/organometallic and organic contaminants at the atmosphere-water-plankton interfaces and through the planktonic food webs, i.e., phyto-, zoo- and bacterio-plankton, with the deep chlorophyll maximum (DCM) as privileged study zone.

3) Implement ultra-clean on-board conditions for the collection and treatment of water and plankton samples for ultra-trace-level analyses of inorganic and organic contaminants.
4) Collect large amounts of plankton, suspended particles, and water (dissolved phase) in the DCM and, in a lesser extent, surface/subsurface waters (0–5 m depth) (Fig. 3). The choice of focusing our sampling on the DCM was motivated by the need to 1) collect a high biomass of plankton from the same location to determine the concentration levels of a wide range of contaminants, and over a broad spectrum of planktonic size fractions, and 2) be located in a relevant area for pelagic trophic interactions in both the coastal and marine areas.
5) Separate these large amounts of plankton and particles into various size fractions (from 0.2 μm to >2000 μm) by filtration or sieving (Fig. 3).
6) Share the size fractioned samples for analysis of a battery of parameters, including (i) contaminants, with trace metals, organometals and metalloids (As, Cd, Cr, Cu, Fe, Hg, MeHg, Mn, Ni, Pb, Sb, Zn, etc.), organic contaminants (PAHs, PCBs, PBDEs, PFASs), radionuclides (^{137}Cs) and microplastics, (ii) biomass, size structure, taxonomy, cytometry, diversity and pigment composition of plankton, and (iii) biogeochemical parameters, with nutrients, total chlorophyll *a* (TChl*a*), suspended particulate matter (SPM), dissolved and particulate organic matter, C and N isotopic ratios (δ^{13}C, δ^{15}N), and biochemical compounds (carbohydrates, proteins, lipids) (Fig. 3).
7) Combine several methods (taxonomy, optical measurements, chemical analyses) to tentatively distinguish the contributions of living (plankton) and non-living (detrital) materials to contaminant accumulation and transfers.
8) Collect on-board samples of atmospheric wet deposition (rain) to assess their potential importance as a source of contaminants for marine water and plankton. The collection of atmospheric samples was also done in parallel on the coast by setting up two ground stations, located in the northern part (Marseille, France) and southern part (Sfax, Tunisia) of the Mediterranean basin (Fig. 2a), in which atmospheric total (dry and wet) deposition were measured on a regular (bi-monthly or monthly) basis from March 2019 to June 2020, i.e., before, during, and after the oceanographic cruise.
9) Sample small pelagic plankton-feeding fishes in Tunisian waters (see sampling positions in Fig. 2a). The fish samples were analysed for a number of contaminants in order to set bioaccumulation factors for higher trophic levels.

2.2. Cruise track and study stations

The MERITE-HIPPOCAMPE cruise took place in spring 2019, from April 13 to May 14, on board the French Research Vessel (R/V) *Antea* along a North-South transect (round trip) in the Mediterranean Sea, from the French coast (La Seyne-sur-Mer, Northwestern Mediterranean) to the Gulf of Gabès in Tunisia (Southeastern Mediterranean) (Tedetti and Tronczynski, 2019) (Fig. 2a, b). Leg 1 (13–28 April 2019) ran the southward transect, between La Seyne-sur-Mer and Tunis, with sampling at five stations: St2, St4, St3, S10, and St11 (in this chronological order). Leg 2 (30 April–14 May 2019) covered first the end of the southward transect (from Tunis to the Gulf of Gabès), and then the return trip back northward from the Gulf of Gabès to La Seyne-sur-Mer. Five stations were sampled during leg 2: St15, St17, St19, St9 and St1 (in this chronological order). Five stations (St1–St4, St9) were situated in the French area, two stations (St10, St11) in the Italian area, and three stations (St15, St17, St19) in the Tunisian area (Fig. 2a, b; Table 1).

The ten stations were chosen according to different criteria based on physical, biogeochemical and biological conditions and anthropogenic pressures (Figs. 2a; S1; Table 1). St1 and St4 were located in the urbanised bays opposite the cities of Toulon and Marseille, respectively, and thus submitted to strong anthropogenic pressures. St4 was the SOLEMIO station, which is part of the French national coastal

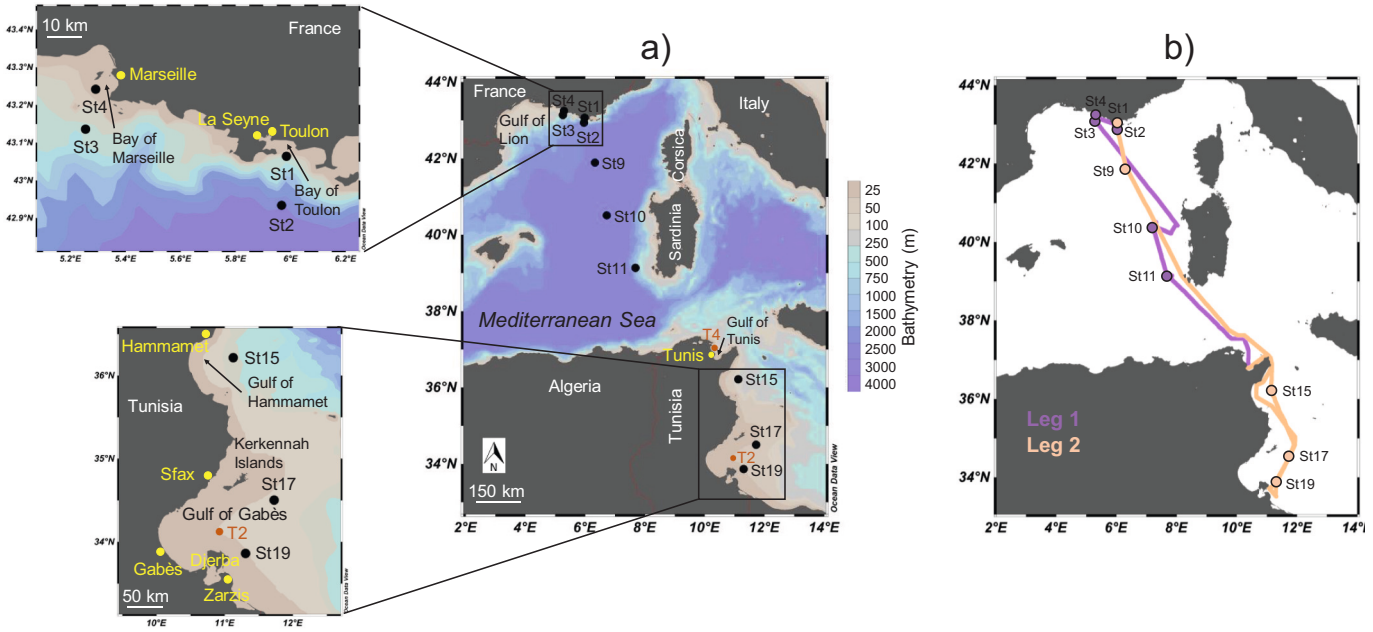

Fig. 2. a) Location of the ten stations (black circles) investigated during the MERITE-HIPPOCAMPE cruise (13 April–14 May 2019) along a North-South transect in the Mediterranean Sea on board the R/V *Antea*. The main characteristics of these stations are provided in Table 1. In addition, two other stations (T2 and T4, brown circles) were sampled in the Tunisian waters during leg 2 (2–3 May 2019) on board the R/V *Hannibal* for trawling of small pelagic fishes (see Table 2 for more details). Two ground stations, located in the northern part (Marseille, France) and southern part (Sfax, Tunisia) of the Mediterranean basin, were set up for the collection of atmospheric deposition samples from March 2019 to June 2020 (i.e., before, during and after the cruise). b) Cruise track with the position of the ten stations studied on board the R/V *Antea*. During leg 1 (13–28 April; from La Seyne-sur-Mer to Tunis), five stations were sampled: St2, St4, St3, S10 and St11 (in this chronological order), while the five other stations were sampled during leg 2 (30 April–14 May; from Tunis to Gulf of Gabès, and then return to La Seyne-sur-Mer): St15, St17, St19, St9 and St1 (in this chronological order). (For interpretation of the references to colour in this figure legend, the reader is referred to the web version of this article.)

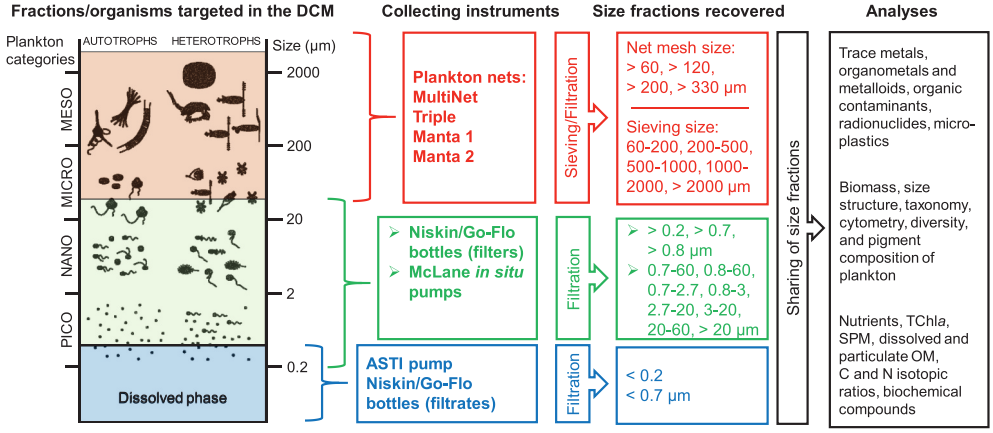

Fig. 3. Summary of our approach with 1) the collection of large amounts of plankton, suspended particles, and water in the deep chlorophyll maximum (DCM) and surface/subsurface waters (0–5 m depth) with various collecting instruments, 2) the separation of these materials into diverse size fractions by sieving or filtration, and the sharing of the obtained size fractions for numerous biological and chemical analyses. Adapted from Alcaraz and Calbet (2003).

observation monitoring network SOMLIT (http://somlit.epoc.u-bordeaux1.fr/fr/). St1 and St4 were "intermittent bloom" areas or "bloom" areas according to D'Ortenzio and d'Alcalà (2009) based on SeaWiFS satellite observations of surface TChl*a* concentration. St2 and St3 were situated offshore of Toulon and Marseille, respectively. St2 was at the limit of the continental shelf and the boundary of the Ligurian consensus region (Ayata et al., 2018) (Fig. S1). St3, situated at the southeast entrance to the Gulf of Lion's continental shelf, was the JULIO station, which is dedicated to the study of intrusions of the Ligurian-Provençal current (Barrier et al., 2016). St2 and St3 were considered "intermittently bloom" areas or "bloom" areas (D'Ortenzio and d'Alcalà, 2009). These stations (St1–St4) have hosted in the past or continue to host visits serving several monitoring networks such as SOMLIT and ROMARIN, and projects including MERMEX-MERITE, COSTAS and IBISCUS.

St9 corresponds to offshore station 1 of the PEACETIME cruise (Guieu et al., 2020). It was located north of the North Balearic thermal Front (NBF), at the boundary of the Ligurian consensus region (Ayata et al., 2018), in the winter convection area (Fig. S1). The NBF, which is one of the main consensus frontiers of the Mediterranean Sea (Ayata et al., 2018), is found between the Balearic Islands and Sardinia, but its position spans a large area and can vary with wind conditions and seasons (Barral et al., 2021). St10 (offshore station 2 of the PEACETIME cruise) was situated south of St9, very close to the NBF. Although St10 was positioned south of the average position of the NBF, it was in fact

Table 1
Main characteristics of the ten stations investigated in spring during the MERITE-HIPPOCAMPE cruise (13 April–14 May 2019) on board the R/V *Antea* along a North-South transect in the Mediterranean Sea. The stations are presented in chronological order in leg 1 then leg 2.

Leg	Station	Latitude (N)	Longitude (E)	Location	Features	Area	Depth (m)	Start of operations (dd/mm in 2019)	End of operations (dd/mm in 2019)
1	St2	42° 56.020′	5° 58.041′	Offshore Toulon	Limit of the continental shelf; Boundary of the Ligurian consensus region[d]; Intermittently bloom area or bloom area (cluster #4 or #5)[e]	French	1770	14/04	16/04
	St4	43° 14.500′	5° 17.500′	Bay of Marseille (SOLEMIO[a] station)	Urbanised bay; Intermittently bloom area or bloom area (cluster #4 or #5)[e]	French	58	16/04	18/04
	St3	43° 08.150′	5° 15.280′	Offshore Marseille (JULIO[b] station)	Southeast entrance to the Gulf of Lion; Intrusions of the Ligurian-Provençal current; Intermittently bloom area or bloom area (cluster #4 or #5)[e]	French	95	18/04	20/04
	St10	40° 18.632′	7° 14.753′	Offshore (station 2 of PEACETIME cruise[c])	Slightly north of the North Balearic Front; Intermittently bloom area (cluster #4)[e]	Italian	2791	22/04	24/04
	St11	39° 07.998′	7° 41.010′	Offshore (station 3 of PEACETIME cruise[c])	South of the North Balearic Front; Algerian consensus region[d]; Presence of mesoscale eddies; No bloom area (cluster #3)[e]	Italian	1378	25/04	26/04
2	St15	36° 12.883′	11° 07.641′	Gulf of Hammamet	Close to the Sicily Channel; Possible entrance of Atlantic Tunisian Current branch; No bloom area (cluster #3)[e]; High density of small pelagic fishes	Tunisian	100	29/04	30/04
	St17	34° 30.113′	11° 43.573′	North of Gulf of Gabès	Gabès consensus region[d] boundary; Shallow area, influence of tides and Atlantic Tunisian Current; Coastal bloom area (cluster #6)[e]; High density of small pelagic fishes	Tunisian	50	01/05	02/05
	St19	33° 51.659′	11° 18.509′	South of Gulf of Gabès	Gabès consensus region[d]; Shallow area, influence of tides and Atlantic Tunisian Current; Coastal bloom area (cluster #6)[e]; High density of small pelagic fishes	Tunisian	50	02/05	05/05
	St9	41° 53.508′	6° 19.998′	Offshore (station 1 of PEACETIME cruise[c])	North of the North Balearic Front; Boundary of the Ligurian consensus region[d]; Winter convection area; Bloom area (cluster #5)[e]	French	2575	08/05	09/05
	St1	43° 03.819′	5° 59.080′	Bay of Toulon	Nearly closed urbanised bay; Intermittently bloom area or bloom area (cluster #4 or #5)[e]	French	91	10/05	11/05

[a] The SOLEMIO station (*Site d'Observation Littoral pour l'Environnement du MIO*) is part of the French national network of coastal observation SOMLIT (*Service d'Observation en Milieu LITtoral* – http://somlit.epoc.u-bordeaux1.fr/fr/).
[b] The JULIO station (*JUdicious Location for Intrusions Observations*) is dedicated to the study of the intrusions of the Ligurian-Provençal current.
[c] The PEACETIME cruise (*ProcEss studies at the Air-sEa Interface after dust deposition in the MEditerranean sea*) took place in May–June 2017 (http://peacetime-project.org/; Guieu et al., 2020).
[d] Consensus regions of the Mediterranean Sea as defined by Ayata et al. (2018).
[e] Bloom/cluster areas as defined by D'Ortenzio and d'Alcalà (2009) from SeaWiFS satellite surface TChl*a* concentration observations.

located slightly north of the front which had moved further south during the sampling period (Rwawi et al., in prep.). St11 (offshore station 3 of the PEACETIME cruise) was plainly positioned south of the NBF, in the Algerian consensus region (Ayata et al., 2018) (Fig. S1). St10 and St11 were characterised by the presence of intense mesoscale eddies: St10 was rather situated between one anticyclonic and one cyclonic eddy, while St11 was located within an anticyclonic eddy (Rwawi et al., in prep.). St9, St10, and St11 are referred to as "bloom", "intermittent bloom" and "no bloom" areas, respectively, according to the D'Ortenzio and d'Alcalà (2009) system (Fig. 2a; Table 1).

St15, situated in the Gulf of Hammamet (Tunisia), was close to the Sicily Channel, which plays host to the exchanges between the two (Western and Eastern) Mediterranean basins, and submitted to the possible entrance of the Atlantic Tunisian Current branch, also called the Atlantic-Ionian stream. St17 (north of the Gulf of Gabès) and St19 (south of the Gulf of Gabès) were located at the boundary of and within the Gabès consensus region, respectively (Ayata et al., 2018) (Fig. S1), and are typified by shallow waters, strong influences of tidal pull (the highest of the Mediterranean; amplitude >2 m) and the Atlantic Tunisian Current. St17 and St19 are also characterised by nutrient inputs from Saharan dust deposition or sediment resuspension and the resulting high planktonic productivity levels (Béjaoui et al., 2019). Moreover, given its cumulative index of warming, overfishing and pollution effects, the Gulf of Gabès has recently been recognised as a hotspot of anthropogenic pressures within the Mediterranean Sea (Reygondeau et al., 2014). St15, St17 and St19 were zones marked by a high density of small pelagic fish and considered as "no bloom" (St15) or "coastal bloom" areas (St17, St19) based on the D'Ortenzio and d'Alcalà (2009) system. These stations (St15-St19) have been investigated in the past in the framework of the Tunisian POEMM and ESSATEL programs (Figs. 2a; S1; Table 1).

Due to rough sea conditions that occurred during sampling of St19 (south of the Gulf of Gabès; Fig. 2a, b), the ship went to shelter, first off the island of Djerba and then off the city of Zarzis (Fig. 2a, b), before returning to station St19 to finish work between May 3 and 4. During the transit between off Djerba and off Zarzis, atmospheric deposition sampling was carried out following an intense episode of Saharan dust deposition.

Besides the ten stations prospected from the R/V *Antea*, two other stations (T2 and T4) were sampled in the Tunisian waters during leg 2 (2–3 May 2019) on board the R/V *Hannibal* for trawling small pelagic fishes. T2 was located in the Gulf of Gabès not far from St19, whereas T4 was situated in the Gulf of Tunis. The duration of trawling was 40 min at T2 and 90 min at T4 (Fig. 2a; Table 2). The fish species captured by trawling were anchovy, sardine, sardinella, and mackerel (Lajnef et al., in prep.).

Table 2
Main characteristics of the two stations investigated during the MERITE-HIPPOCAMPE cruise in May 2019 on board the R/V *Hannibal* in the Tunisian waters for trawling of small pelagic fishes.

Station	Latitude (N)	Longitude (E)	Location	Depth (m)	Date (dd/mm in 2019)	Trawling duration
T2	34° 11.892′	10° 58.152′	Gulf of Gabès	45	02/05	0 h40
T4	36° 59.142′	10° 19.734′	Gulf of Tunis	37	03/05	1 h30

2.3. Equipment and operations

At each of the ten stations, the following sampling equipment was deployed and the following operations were performed at sea and on board the R/V *Antea*.

2.3.1. Water sampling with Niskin and Go-Flo bottles and subsequent in-line filtration

A trace metal-clean carousel equipped with ten 12-L bottles (1 Niskin, 5 Niskin X, 4 Go-Flo) and a conductivity-temperature-depth probe (CTD; Seabird SBE 911*plus*), mounted with photosynthetically available radiation (PAR) (Biospherical), TChl*a* fluorescence (Aqua Tracka, Chelsea ctg), dissolved oxygen (O_2) (SBE 43), dissolved organic matter (DOM) fluorescence (WETStar, WETLabs) and transmittance (C-Star, WETLabs) sensors, was deployed from the ship's moon pool via the electro-mechanical (conducting) cable (Table S1; Fig. S2a). Vertical profiles were collected over the depth range 0–250 m or surface-to-bottom when depth was <250 m, and seawater was sampled at two depths: 5 m or the DCM identified based on TChl*a* profiles. Seven bottles (4 Niskin X and 3 Go-Flo) were dedicated to DCM sampling, while three bottles (1 Niskin, 1 Niskin X and 1 Go-Flo) were used for 5-m-depth sampling. The Go-Flo bottles were lowered into the water in open position. At St9 and St10, sampling was also conducted down to 500-m depth to collect seawater in the oxygen minimum zone (OMZ) identified based on O_2 profiles. At St9, water was collected at 5 m, DCM and 440 m (identified as OMZ), whereas at St10 sampling was carried out at 5 m, DCM, 100, 200, 300, 400 m (identified as OMZ) and 500 m. The Niskin X bottles used here (model 101,012×) are Niskin with a completely free Teflon-coated sample chamber, Teflon-coated and externally-located stainless steel end plug closure springs, as well as Teflon-coated air valves and drainage taps. Before the cruise, all ten bottles were thoroughly washed with hydrochloric acid (HCl) 1 M, demineralized water and ultra-pure water (i.e., Milli-Q water from Millipore system, final resistivity of 18.2 MΩ cm). Before sampling, they were rinsed with seawater collected at 50-m and 170-m depth at the first station (St2). Between two casts, working on the deck of the ship, we covered the drainage taps and the top (upper stoppers) of the bottles with plastic bags to avoid any sample contaminations.

Once on board, after water collection at 5-m depth and in the DCM, the carousel with all the bottles was placed in the wet laboratory for in-line filtration (Table S1; Fig. S2b). For that purpose, the bottles were pressurised to 0.5 bar with argon (UN1006, compressed, 2.2) piped in using a silicon tubing system and quick-connect gas fittings replacing bottle air valves. The upper and lower stoppers of the Niskin bottles were held tight by home-made pairs of high-density polyethylene (HDPE) rods and clamps screwed at the top and bottom. A 10-cm-long piece of acid-cleaned silicon tubing was inserted into the drainage tap of each bottle, and a perfluoroalkoxy (PFA) filter holder (Savillex®, 25 or 47-mm diameter) was connected to the tubing. A graduated container collecting the filtered water served to indicate the exact volume filtered on each filter.

In-line filtration makes it possible to effectively filter large quantities of water in clean conditions and to recover the filters and filtered water samples for a battery of analyses. Filtration was done on pre-combusted (450 °C, 6 h), pre-weighed glass fibre filters (GF/F, Whatman) of 25 or 47-mm diameter (pore size: ~ 0.7 μm) for analyses of TChl*a*, pigments, SPM, particulate organic carbon (POC), particulate organic nitrogen (PON), stable isotopes of carbon and nitrogen ($\delta^{13}C$, $\delta^{15}N$), biochemical compounds (carbohydrates, lipids, proteins) and Hg on the size fraction >0.7 μm. SPM measurements were done on (pre-weighed) 25-mm and 47-mm-diameter GF/F filters rinsed with ultra-pure water after filtration in order to remove salts, but also on (pre-weighed) 47-mm-diameter GF/F filters that had not been rinsed with ultra-pure water (for which the amount of salts was estimated). Filtration was also done on pre-cleaned 0.2-μm-pore-size 47-mm-diameter mixed cellulose esters (MCE) filters for the analyses of trace metals/metalloids and microbial diversity on the size fraction >0.2 μm, and on 0.8-μm-pore-size 47-mm-diameter pre-cleaned MCE filters for the analyses of copper (Cu) and zinc (Zn) isotopes on the size fraction >0.8 μm. GF/F-filtered seawater (< 0.7 μm) was used for the analyses of nutrients, i.e., silicates [$Si(OH)_4$], nitrates (NO_3^-), nitrites (NO_2^-), phosphates (PO_4^{3-}) and ammonium (NH_4^+), dissolved organic carbon (DOC), and absorption of chromophoric DOM (a_{CDOM}), whereas 0.2-μm-filtered seawater was used for the analyses of dissolved trace metals/metalloids and Hg (Fig. 3; Table S1). Volume of seawater filtered ranged from 600 mL (25-mm GF/F filter for TChl*a*) to 12 L (47-mm GF/F filter for POC, PON, $\delta^{13}C$, $\delta^{15}N$, and biochemical compounds).

Raw (unfiltered) seawater was taken for the analyses of total trace metals/metalloids and Hg/MeHg, while seawater pre-filtered onto 100-μm silk was collected for phytoplankton taxonomy and cytometry analyses. Raw seawater from the DCM was also used to perform on-board experiments on microbial methylation/demethylation of Hg (at selected stations), while raw seawater collected at 5-m depth and in the DCM at St1, St9, S15 and St19 was used to conduct dilution experiments (see Section 2.3.8). Most of these filtrations were also conducted on OMZ water (at St9 and St10) for the same analyses. Raw and 0.2-μm-filtered seawater at the different depths was also used for shipboard analyses of Hg (see Section 2.3.9) (Table S1). Filter blanks were regularly run during the cruise: filters were treated as sample filters, either without passing any water on them or by rinsing with ultra-pure water, depending on the parameter. Detailed information on the in-line filtration from Go-Flo and Niskin bottles, including storage of samples, can be found in Fig. S3.

2.3.2. In situ optical measurements

A small CTD unit (SBE 19*plus*) equipped with a TChl*a* fluorescence sensor (WETStar, WETLabs) was deployed from the moon pool on the hydrographic cable, over the same depth range as the carousel (0–250 m or 0–bottom), to timely determine the depth of the DCM between different sampling operations, in particular just before McLane in situ pumps (see Section 2.3.3) and MultiNet deployments (see Section 2.3.5) (Table S1).

A laser optical plankton counter (LOPC, Rolls Royce) and laser in situ scattering transmissometry-Holography (LISST-HOLO, Sequoia Scientific) were used together, fixed on a small carousel, to provide information on the abundances and size spectra of particles and plankton (> 20 μm for LISST-HOLO, > 100 μm for LOPC). Both systems were deployed from the moon pool on the hydrographic cable. Vertical profiles were performed over the depth range 0–250 m or 0–bottom (Table S1; Fig. S2c).

2.3.3. In situ filtration with McLane pumps

Four McLane Large Volume Water Transfer System Samplers (WTS6-142LV, 4–8 L min^{-1}), hereinafter referred to as McLane in situ pumps, were used to collect large amounts of particles and plankton over different size fractions in the DCM. The four pumps were attached together with clamps and chains, and deployed at the same time from the moon pool on the hydrographic cable to reach the DCM (Fig. S2d). Pumping lasted between 40 and 60 min, giving an average ~ 240 L of water filtered by each pump. Three successive casts of the four-pump system were carried out, giving a total of 12 pumping runs done at

each station (Table S1).

Three pumps (A, B, C) were each mounted with a regular 142-mm filter-holder ("McLane holder") holding one 142-mm-diameter filter: one ~0.7-μm-pore-size pre-combusted pre-weighed GF/F filter, one 0.8-μm-pore-size pre-cleaned MCE filter, or one 20-μm-pore-size pre-cleaned Nylon filter. After installing the filters, the three McLane holders were covered with a 60-μm-pore-size sock-type pre-filter so that the filtered particles size fractions were 0.7–60, 0.8–60 and 20–60 μm. At three casts each, pumps A, B and C were able to sample nine filters for analysis of TChl*a*, SPM, POC, PON, $\delta^{13}C$, $\delta^{15}N$, biochemical compounds, PAHs, PCBs, PBDEs and Hg/MeHg on the GF/F filters (0.7–60-μm size fraction), analysis of trace metals/metalloids, Cu and Zn isotopes and microbial diversity on the MCE filters (0.8–60-μm size fraction), and analysis of microplastics on the Nylon filters (20–60-μm size fraction) (Figs. 3; S4; Table S1).

The fourth pump (D) was mounted with a mini-Multiple Unit Large Volume in-situ Filtration System (MULVFS) filter holder composed of baffle tubes on the top followed by successive baffle and filter support plates, for sequential filtration with three different filters (142-mm diameter) (Bishop and Wood, 2008; Bishop et al., 2012). The baffles were designed to straighten the flow, suppress turbulence, and distribute particles evenly across the filter. The filter series used were either 1) one ~0.7-μm-pore-size pre-combusted, pre-weighed GF/F filter, one 2.7-μm-pore-size pre-combusted, pre-weighed GF/D filter, and one 20-μm-pore-size pre-cleaned Nylon filter, or 2) one 0.8-μm-pore-size pre-cleaned MCE filter, one 3-μm-pore-size pre-cleaned MCE filter, and one 20-μm-pore-size pre-cleaned Nylon filter. With its three casts, pump D was able to collect nine filters for the analysis of TChl*a*, SPM, POC, PON, $\delta^{13}C$, $\delta^{15}N$, biochemical compounds, and Hg/MeHg on the 0.7–2.7, 2.7–20, and > 20-μm size fractions, and trace metals/metalloids on the 0.8–3, 3–20, and > 20-μm size fractions (Figs. 3; S4; Table S1).

SPM measurements were made on (pre-weighed) 142-mm GF/F, GF/D and Nylon filters rinsed with ultra-pure water after filtration in order to remove residues of the seawater salts, but also on (pre-weighed) 142-mm GF/F filters not rinsed with ultra-pure water (for which the amount of salts was estimated). All filters were placed in glass boxes, plastic boxes or aluminium foil, depending on the parameter, and stored on board at −20 °C (Figs. S2e, f; S4). A special support was purpose-designed to accommodate/fix the filter holders in the wet laboratory to facilitate the process of preparing the filters before deployment, and then handling, rinsing with ultra-pure water or direct drying (by connecting the filter holder to a vacuum pump) the filters after deployment (Fig. S2e, f). Before pump deployment, all the filter holder and filter systems were rinsed with ultra-pure water. Filter blanks were done at regular intervals during the cruise.

2.3.4. Water sampling and subsequent in-line filtration with an ASTI pump

Seawater was also sampled at ~10–20-m depth with a pneumatically-operated Teflon ASTI pump (model PFD2) set up on board and connected to Teflon tubing, which was weighted down and immersed from port side with the hydrology gallows (Table S1). The pumped seawater was filtered in-line onto a pre-combusted 142-mm GF/F filter using a 142-mm Teflon filtration holder. This filtration took place in the clean lab container (IFREMER, CNXU 300022/1) installed on the rear deck of the ship. Part of the filtered seawater was stored in three 20-L stainless steel jerrycans, while the other part was stored in a metal-free 50-L plastic container. This filtered seawater was used for sieving the large quantities of plankton collected with the Multiple Plankton Sampler. The filtered seawater stored in two of the stainless steel jerrycans was used exclusively for sieving on a stainless steel sieve column to obtain plankton samples for organic parameter analyses, and the filtered seawater stored in the plastic container was used exclusively for sieving on a nylon sieve column for analyses of inorganic parameters (see Section 2.3.5). Filtered seawater from the third jerrycan was amended with 50 mL of dichloromethane, then shaken and degassed and stored in the container at ambient temperature for subsequent analyses of dissolved (< 0.7 μm) hydrocarbons (Guigue et al., in prep.) (Fig. 3; Table S1). All seawater containers (stainless steel and plastic) were rinsed several times with filtered seawater before sample collection.

2.3.5. Plankton sampling with a MultiNet and subsequent sieving

A Multiple Plankton Sampler (Midi type, Hydro-Bios), referred to hereafter as "MultiNet", was employed to collect plankton in the DCM. The MultiNet was composed of 5 individual (exchangeable) 2.5-m-long nets with 0.25-m^2 apertures, a 60-μm mesh size, and cod ends of the same mesh size, together with two Hydro-Bios flowmeters (one into the mouth and the other on the side) to assess the volume of water filtered by the nets, plus a CTD sensor and a TChl*a* fluorometer (Chelsea ctg). The MultiNet was connected via the electro-mechanical cable to the operating computer to enable online monitoring of sensor feedback and opening and closing of the nets, mainly based on flowmeter data and the amount of water passing through the open net. It was operated from the stern A-frame. Since the device was deployed horizontally in the DCM, the usual configuration (for vertical casts) was modified with a V-fin deflector attached below the MultiNet and the five cod ends attached using a helicoidal bucket connector (Fig. S2g, h). Ship speed while towing the MultiNet was ~2 knots (Table S1). Once the five nets were filled (after 30 to 100 min depending on the station), the MultiNet was hauled back on board, the cod ends were rinsed out with local seawater, and their content was transferred to pre-cleaned 10-L HDPE bottles. The instrument was then returned to the water. This operation ("cast") had to be repeated several times (between two and eight horizontal casts, depending on the station) until we got sufficient amounts of plankton. At St19, due to technical issues, the MultiNet was replaced by a square net with a 1-m^2 aperture mounted with single 60-μm mesh-size net. Total filtered water volume with the MultiNet/square net ranged from 314 (St2) to 2373 m^3 (St10).

In the clean on-board container lab, plankton collected in HDPE bottles was then size-fractionated on 1) a column of five stainless steel sieves (60, 200, 500, 1000 and 2000-μm mesh-size) by wet-sieving with the GF/F filtered seawater stored in stainless steel jerrycans for subsequent analyses of organic parameters, and 2) a column of five nylon sieves (60, 200, 500, 1000 and 2000-μm mesh-size) by wet-sieving with the GF/F filtered seawater stored in the plastic container for the subsequent analyses of inorganic parameters (Fig. S2i, j). The filtered seawater was routed with a gentle flow to the top of the sieve column by the ASTI pump using Teflon tubing. The plankton size fractions recovered on the stainless-steel sieves were shared out and transferred to pre-combusted glass flasks for the analyses of POC, PON, $\delta^{13}C$/$\delta^{15}N$, biochemical compounds, PAHs, PCBs, PBDEs and PFASs, or to plastic flasks for zooplankton taxonomy and imagery, TChl*a* (60–200-μm size fraction only) and microbial diversity (60–200 and 200–500-μm size fractions only). The plankton size fractions recovered on the nylon sieves were shared out and transferred to pre-cleaned polypropylene flasks for the analyses of trace metals/metalloids, Hg and ^{137}Cs (Figs. 3; S5; Table S1). Planktonic biomass (in mg m^{-3} dry weight) was also determined in each of the size fractions (Fierro-González et al., 2023). All samples were stored at −20 °C except those for zooplankton taxonomy that were stored at ambient temperature after adding buffered formalin (Fig. S5).

2.3.6. Plankton and micro-plastic sampling with triple and Manta nets

A triple net, equipped with 60, 120 and 200-μm mesh-sized nets each with 0.60-m aperture diameter was used to undertake two vertical tows over the depth 0–200 m (or 0–bottom if depth < 200 m), i.e., one tow for biomass, and one tow for taxonomy and imagery. The device was deployed from port side using hydrology gallows (Table S1; Fig. S2k). After collection, the cod-end contents from each of the three nets (first tow) were passed through GF/F filters that were stored in Petri dishes at −20 °C for biomass measurements, while the cod-end contents from the second tow were passed through a 60-μm sieve for volume reduction and

transferred to 250-mL plastic tubes amended with 12.5-mL buffered formalin for taxonomy and imagery analyses. At St1, St9, S15 and St19, the contents of the 200-μm net were also collected to analyse chlorophyll gut-contents of mesozooplankton (see Section 2.3.8).

Two Manta nets were used for horizontal tows in surface waters: one a 330-μm mesh size (1 tow, 3 knots, 20 min max) for microplastic analyses, and the other a 60-μm mesh size (1 tow, 1 knot, 10 min max) for microplastics and plankton (neuston) analyses, both deployed from port side using hydrology gallows (Table S1). After collection, the content of the 330-μm Manta net was sieved successively through 5000 and 300-μm mesh-size sieves (if large items were present in the collectors) and transferred to a 1-L glass bottle added with formalin (4 % final concentration). The content of the 60-μm Manta net was transferred to a 1-L glass bottle added with 50-mL buffered formalin.

2.3.7. In-line filtration onto cartridges

At each station, in-line filtration was carried out in the wet laboratory on seawater collected continuously at 2-m depth by the shipboard pump system (Table S1). Two polypropylene cartridges (Polycap HD), the first with a 20-μm pore size and the second with a 0.45-μm pore size, were mounted in series to recover the 0.45–20-μm and > 20-μm size fractions. Around 1000 L of seawater was filtered on the two cartridges at each station. The dissolved fraction (< 0.45 μm) was collected in 20-L plastic containers. These samples served for radionuclide analyses (^{137}Cs) (Radakovitch et al., in prep.).

2.3.8. Dilution experiments

At St1, St9, S15 and St19, seawater collected from the carousel bottles at 5-m depth and in the DCM was used to perform dilution experiments by means of a thermostatic incubation chamber (Table S1). These experiments were implemented to assess the phytoplankton production rates and microzooplankton grazing rates. At the same stations, the contents of the 200-μm Triple nets (vertical tows) were used to analyse the chlorophyll gut contents of mesozooplankton by fluorescence in order to estimate the impact of mesozooplankton grazing on large phytoplankton (i.e., nano- and micro-phytoplankton). These experiments and measurements served to determine the carbon fluxes and type and structure of the planktonic food webs (Medebb et al., in prep.).

2.3.9. Shipboard analyses

Unfiltered and 0.2-μm-filtered seawater collected from the carousel bottles at 5-m depth, in the DCM and at the other depths (profiles, OMZ) served for shipboard analyses of total and purgeable Hg using a Tekran® auto-analyser (model 2500), consisting in purge and trap of volatilized Hg species followed by cold vapour atomic fluorescence spectrometry (CVAFS) detection (Table S1; Fig. S2m).

A part of the seawater collected continuously at 2-m depth by the shipboard pump system was subsampled and routed to a CytoSense® automated flow cytometer (CytoBuoy) installed in the dry laboratory. The CytoSense was employed to analyse (in terms of identification and abundance) individual or colonial phytoplankton cells sized between 0.8 and 800 μm. Cytometry measurements were carried out continuously at the different stations but also all along the transect (Table S1; Fig. S2l; Boudriga et al., 2022).

2.3.10. Atmospheric deposition

During the cruise, wet atmospheric deposition samples were collected using two rain collectors placed in PVC pipes that were fixed at the front of the ship (10 m above sea level). The collector for trace metal samples was composed of an acid pre-cleaned, metal-free plastic bottle and funnel (Fig. S2n). The collector for PAH samples was composed of a pre-combusted amber glass bottle and glass funnel (Table S1; Fig. S2o). Overall, six rainwater samples were collected (Table 3): two at St10 (Rains 1 and 2), one at St11 (Rain 3), one at St19 (Rain 4), one during the transit from off Djerba island to off Zarzis city (Rain 5, south of St19; Fig. 2a, b) (for both collectors), and one at St1 (Rain 6 only in the PAH collector). The "transit to Zarzis" sample was collected as a result of a dry deposition episode (intense Saharan dust event). In this case, ultrapure water was used to rinse the plastic and glass funnels in order to retrieve all the dry fraction that had settled onto them. Atmospheric samples collected during the cruise were frozen and stored at −20 °C (for PAHs) or at 4 °C (for metals/metalloids), then filtered (at 0.2 or 0.7 μm) in the laboratory to separate dissolved and particulate phases before treatments and analyses. Atmospheric forecast bulletins were regularly sent to the on-board team to anticipate these rain events. Detailed information on the rain samples collected during the cruise can be found in Table 3.

Glass collectors were also set up in two ground stations located in the northern part (Marseille, France) and southern part (Sfax, Tunisia) of the Mediterranean basin (Fig. 2a; Fig. S2p) for sampling total (dry and wet) atmospheric deposition and running the subsequent PAH analyses. This sampling was done on a regular basis (bi-monthly, monthly, or daily in the case of strong rainfall events) from March 2019 to June 2020, i.e., before, during, and after the cruise (Poindron et al., in prep.).

2.3.11. On-vessel scientific equipment and continuous measurements

Subsurface temperature and salinity were recorded continuously at high frequency all along the transect from flow-through pumped seawater at 2-m depth, using a thermosalinograph (TSG, SeaBird SBE 21). A weather station (Batos 1.1 D, Météo France) continuously recorded atmospheric parameters (temperature, wind, pressure, humidity, PAR).

2.4. The sequence of operations and main parameters analysed on the different size fractions

The typical sequence of at-sea/on-board operations conducted from the R/V *Antea* at each station is given in Table S2. The whole sequence of operations at each station lasted 48 h on average but varied depending on meteorological conditions encountered and occasional technical problems. The detailed sequence and timing of the main operations performed during the whole cruise are presented in Table S3, and the total number of operations completed is provided Table S4. Table S5 reports the time and depth of sampling (mostly in the DCM) at each station for the three main operations at sea: the water sampling with the carousel/Niskin and Go-Flo bottles, in situ filtration with the McLane pumps, and plankton sampling with the MultiNet. Table S6 summarises the main parameters analysed on the different size fractions (from <0.2 to >2000 μm) recovered from filtration and sieving after the collecting

Table 3
Information about wet (rain) atmospheric deposition samples collected on board the R/V *Antea* during the MERITE-HIPPOCAMPE cruise.

Sample	Station	Start date of sampling	Start time of sampling (UT)	End date of sampling (dd/mm in 2019)	End time of sampling (UT)	Type of deposition
Rain 1	St10	22/04/19	19 h15	23/04	9 h45	Rain
Rain 2	St10	24/04/19	7 h30	24/04	12 h30	Rain
Rain 3	St11	26/04/19	3 h15	26/04	12 h00	Rain
Rain 4	St19	03/05/19	5 h45	03/05	14 h00	Rain
Rain 5	Transit from off Djerba to off Zarzis	03/05/19	16 h45	04/05	9 h00	Dry deposition + rain
Rain 6	St1	11/05/19	3 h00	11/05	6 h15	Rain

large amounts of plankton, particles, and water in the DCM and surface/subsurface waters (0–5 m depth), i.e., 1) contaminants, with trace metals, organometals and metalloids (As, Cd, Cr, Cu, Fe, Hg, MeHg, Mn, Ni, Pb, Sb, Zn, etc.), organic contaminants (PAHs, PCBs, PBDEs, PFASs), radionuclides (^{137}Cs) and microplastics, 2) plankton biomass, size structure, taxonomy, cytometry, diversity, and pigment composition, and 3) biogeochemical parameters, including nutrients [$Si(OH)_4$, NO_3^-, NO_2^-, NH_4^+, PO_4^{3-}], TChl*a*, SPM, dissolved and particulate organic matter (POC, PON, DOC, a_{CDOM}), C and N isotopic ratios ($\delta^{13}C$, $\delta^{15}N$), and biochemical compounds (carbohydrates, proteins, lipids).

3. Environmental context during the cruise

3.1. Meteorological context

Atmospheric deposition is known to be an external source of metals and PAHs (Castro-Jiménez et al., 2012; Jordi et al., 2012; Desboeufs et al., 2022) as well as of nutrients (Guieu et al., 2020) for Mediterranean surface seawater. The cruise was conducted during the spring, when dust deposition events were commonplace in the Western Mediterranean (Guieu et al., 2020). During the cruise, the Aerosol Optical Depth (AOD) maps derived from the Spinning Enhanced Visible and InfraRed Imager (SEVIRI) satellite instrument (https://www.icare.univ-lille.fr/data-access/browse-images/geostationary-satellites/; Thieuleux et al., 2005) highlighted two dust transports with high AOD (> 0.8) through the Mediterranean Sea: one that occurred between 17 and 26 April 2019 (Figs. 4a; S6) and a second that occurred between 3 and 4 May 2019 (Figs. 5a; S7). These events were associated with significant cloud cover (Figs. 4b, 5b). The Non-hydrostatic Multiscale Model/Barcelona Supercomputing Centre (NMMB/BSC)-Dust model and NASCube (http://nascube.univ-lille1.fr/; Gonzalez and Briottet, 2017) confirmed the emission and export of dust plumes from North Africa to over the Western Mediterranean. The atmospheric dynamics and patterns of the first event are described in detail in Calidonna et al. (2020). This event was associated with a northward atmospheric flux loaded by dust emission from Algeria and southern Morocco. The second dust plume was transported from Algeria and Tunisia by north-eastward winds (not shown).

For the April event, dust plume transport was mainly associated with wet deposition from NMMB/BSC-Dust model forecasts, in agreement with the intensely cloudy conditions (Fig. 4c, d). The geographic range of dust deposition events covered a region from the Balearic basin to the Tyrrhenian Sea and then the Ligurian Sea (Fig. 4a–d), i.e., the vicinity of R/V's locations during St10 and St11 between 20 and 23 April and then on 25 April along the Western coastline of Sardinia (Table 1). The model predictions were confirmed by visual on-board observations of precipitations around and above the R/V's location, corresponding to the first three rain samples (Rains 1, 2 and 3) (Table 3). Note that wet dust deposition started from the afternoon of 22 April after the R/V's arrival on St10, thus ruling out a direct impact of dust deposition on the first cast completed at this station. However, rain events probably impacted surface waters over a large region around the R/V's location during St10 and St11.

For the event in May, NMMB/BSC-Dust model forecasts point mainly to dry dust deposition occurring between 3 and 4 May over the Gulf of Gabès and the Libyan coast (Fig. 5c, d). During this event, the R/V was at St19 in the southern Gulf of Gabès then in transit to Zarzis (Tables 1; S3). Dry dust deposition was confirmed by visual observations of dusty sky and substantial deposited dust material on the decks of the R/V between 3 and 4 May. The Rain 5 sample was collected during this event (Table 3). The inflow of desert dust was also consistent with the highest temperatures and lowest pressures recorded by ship's permanent instrumentation (Fig. S8). It is therefore very likely that this event represented a supply of metal-bearing dust to the surface waters.

Outside of these desert dust transport periods, Hybrid Single-Particle Lagrangian Integrated (HYSPLIT) back trajectories modelling showed that the air masses around the R/V position came from Europe (not shown). Nevertheless, no intense pollution event was either observed or predicted during the cruise from satellite or model outputs. Moreover, no volcanic emissions from Etna were recorded during the cruise.

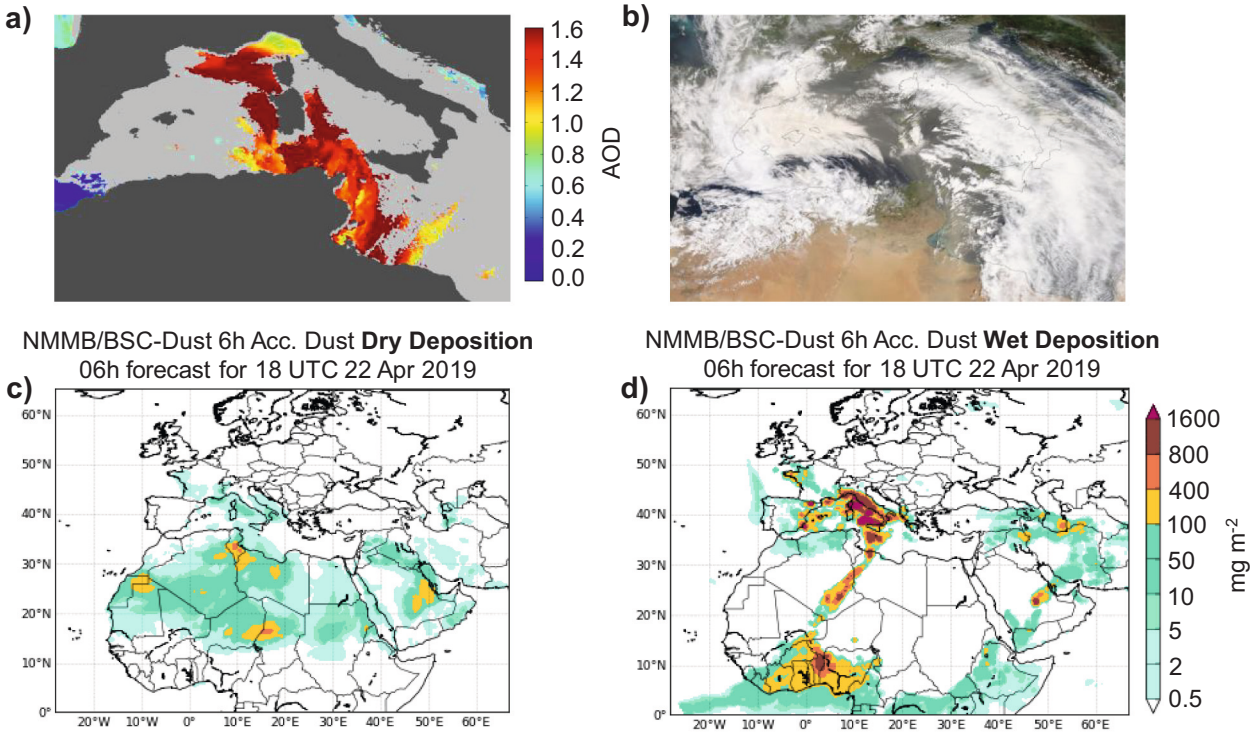

Fig. 4. Saharan dust event of April. Here is presented for 22 April 2019 which is the day where the dust plume was the most intense: a) Daily Aerosol Optical Depth (AOD, unitless) product from MSG-SEVIRI, b) MODIS image from NASA worldview, and BSC-DREAM-Dust forecast of c) dry and d) wet deposition (in mg m^{-2}).

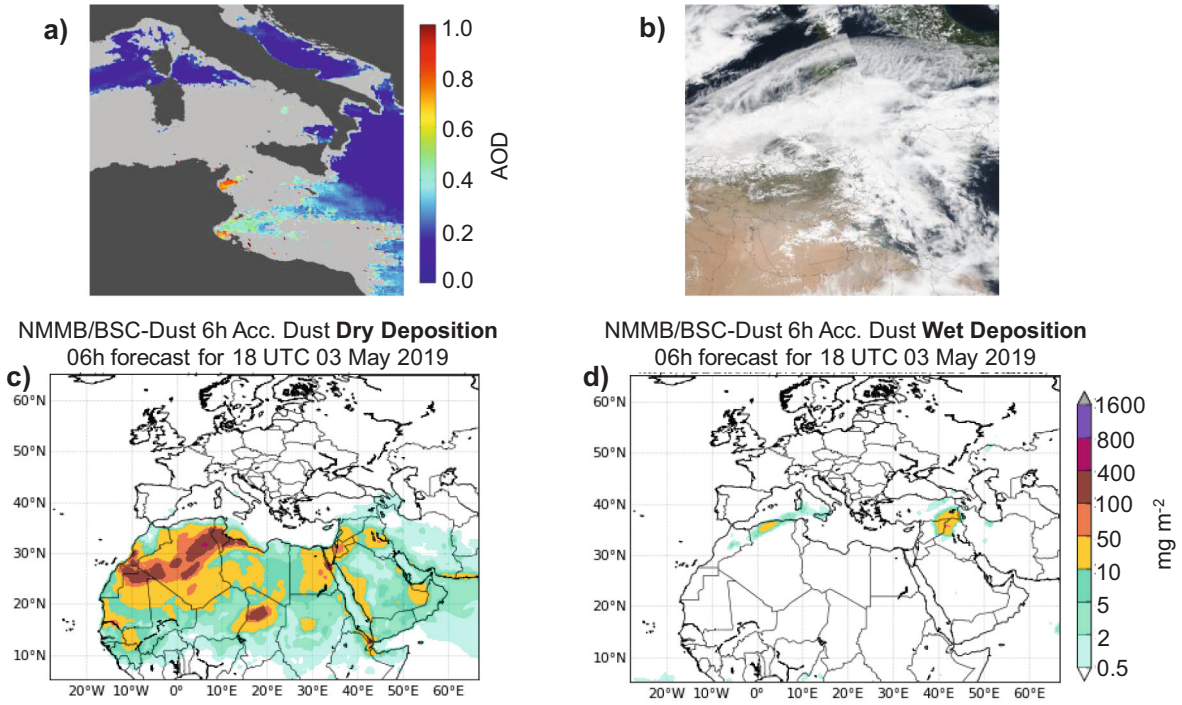

Fig. 5. Saharan dust event of May. Here is presented for 3 May 2019 which is the day where the dust was located over ship's position: a) Daily Aerosol Optical Depth (AOD, unitless) product from MSG-SEVIRI, b) MODIS image from NASA worldview, and BSC-DREAM-Dust forecast of c) dry and d) wet deposition (in mg m^{-2}).

3.2. Hydrological context

Subsurface (2-m depth) temperature gradually increased from north to south of the transect, whereas subsurface salinity decreased from North to South but increased again at the extreme south of the transect (Gulf of Gabès) (Fig. 6). The lowest subsurface temperatures (~ 14.0 °C) were recorded in the Bay of Marseille, while the highest subsurface temperatures (19.5 °C) were observed in the south of the Gulf of Gabès, near Djerba and Zarzis. The highest subsurface salinity values were found in the Ligurian region (38.5) and the lowest (37.1) in the northern Tunisian coastal waters, particularly in the Gulf of Tunis (Figs. 2a, 6; Fig. S1). Because of the vast and contrasted area covered by the cruise, CTD profiles displayed huge variability with depth in temperature and salinity and in TChl*a* and dissolved O_2 concentrations between stations (Figs. 7, 8). Despite this high variability, some similarities emerged. For the stations off French shores (St1–St4), temperature, salinity and TChl*a* values over the water column ranged from 13.6 to 14.9 °C, 37.8–38.4 and 0.02–0.86 μg L^{-1}, respectively, with a slight decrease in temperature and a slight increase of salinity toward the bottom (Fig. 7). Offshore stations (St9–St11) also showed a decrease in temperature and increase

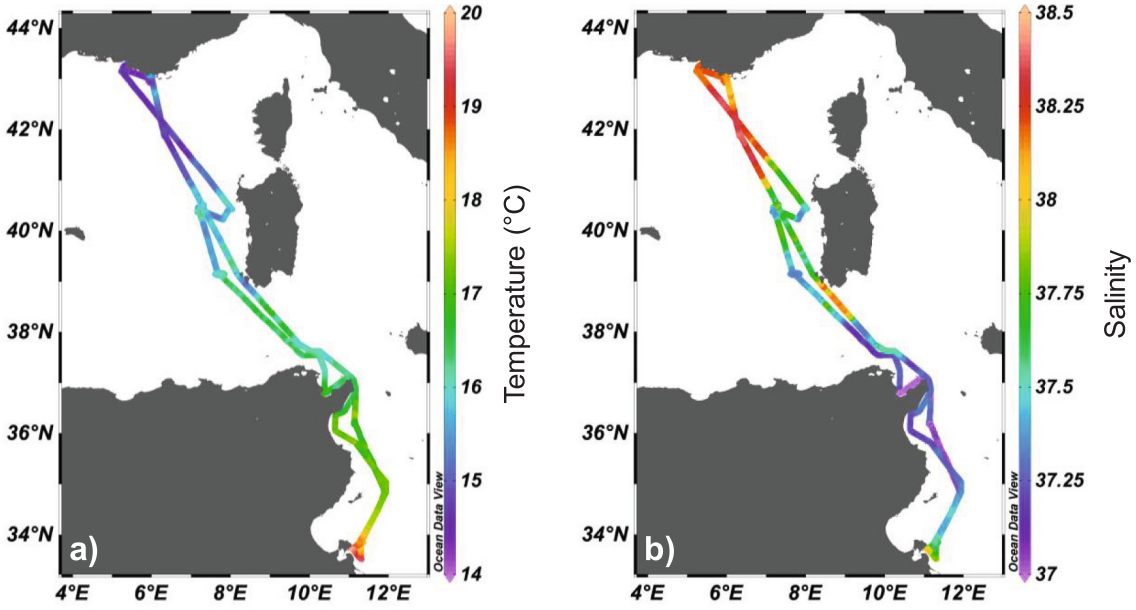

Fig. 6. Distribution of subsurface a) temperature (°C) and b) salinity along the North-South Mediterranean transect recorded continuously from the flow-through pumped seawater at 2-m depth. Ocean Data View (ODV) software version 4.6.5. Schlitzer, R., http://odv.awi.de. Schlitzer, 2014.

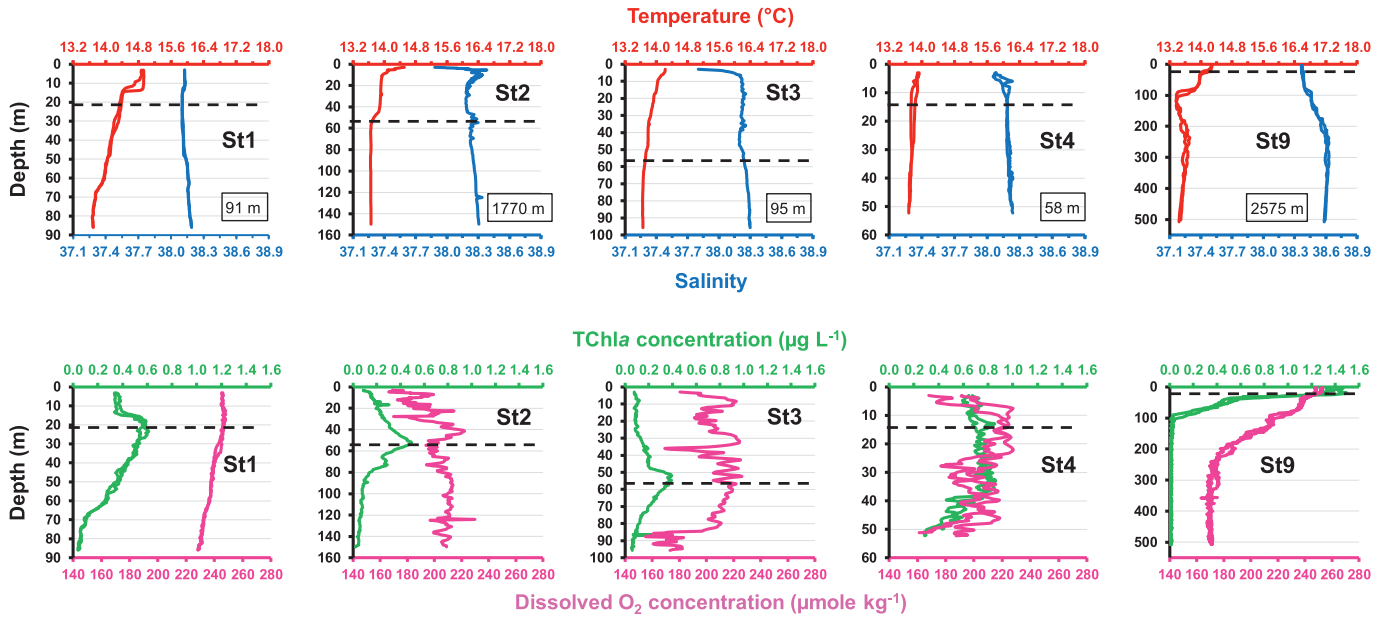

Fig. 7. Vertical profiles of temperature (°C), salinity, TChl*a* concentration (µg L^{-1}) and dissolved O_2 concentration (µmole kg^{-1}) issued from the main carousel CTD deployments (Seabird SBE 911*plus*) at stations St1–St9. The dotted lines represent the depth of sampling in the deep chlorophyll maximum (DCM) for Niskin/Go-Flo bottles. In box, the depth of the station. One or two profiles are displayed for each station. For each profile, only data acquired during the upcast are presented.

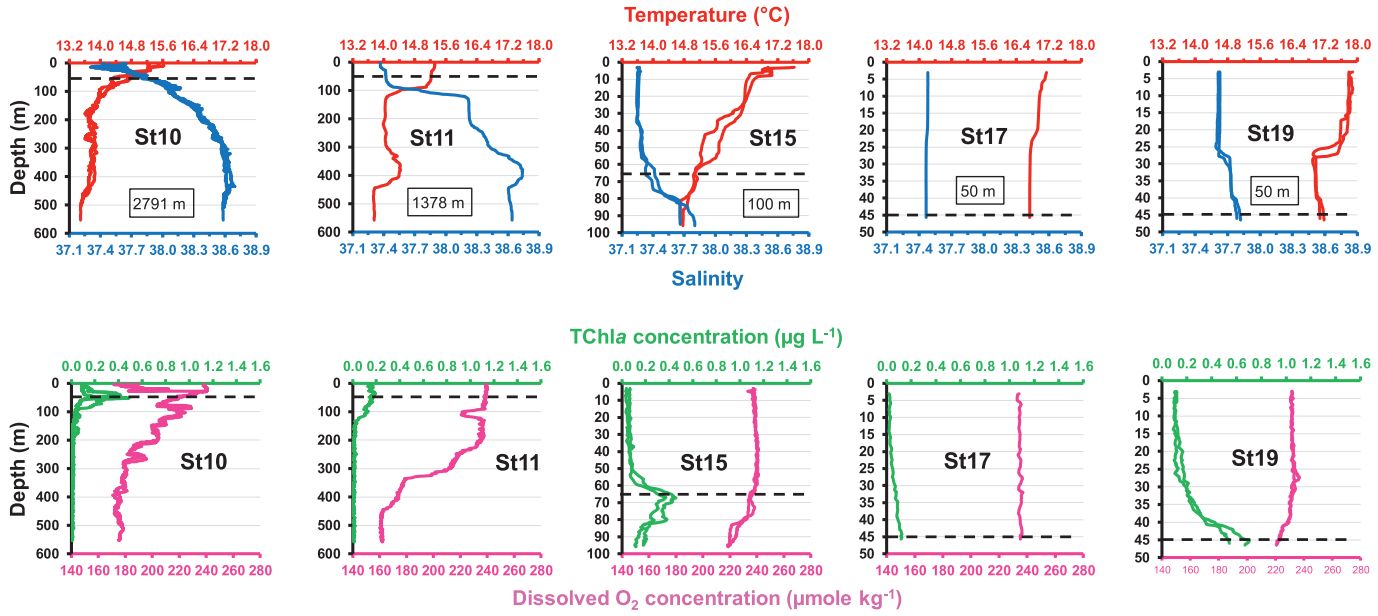

Fig. 8. Vertical profiles of temperature (°C), salinity, TChl*a* concentration (µg L^{-1}) and dissolved O_2 concentration (µmole kg^{-1}) issued from the main carousel CTD deployments (Seabird SBE 911*plus*) at stations St10–St19. The dotted lines represent the depth of sampling in the deep chlorophyll maximum (DCM) for Niskin/Go-Flo bottles. In box, the depth of the station. One or two profiles are displayed for each station. For each profile, only data acquired during the upcast are presented.

of salinity with depth, but with a greater range of variation (compared to the stations along the French coast) in terms of temperature (13.4–15.5 °C), salinity (37.3–38.7) and TChl*a* concentrations (0.00–1.49 µg L^{-1}) with manifestly deeper thermoclines and haloclines (Figs. 7, 8). TChl*a* concentrations were particularly high at St9 (Fig. 7). St11 was marked by a significant increase in both temperature and salinity between 200 and 400 m followed by a decrease between 400 and 430 m before remaining stable down to the bottom (Fig. 8). Tunisian stations (St15–St19) showed higher water column temperatures (14.7–17.9 °C) and lower salinities (37.2–37.8) compared to stations further north, in accordance with subsurface data (Fig. 6), and lower TChl*a* concentrations (0.02–0.70 µg L^{-1}) compared to the northernmost stations. At these Tunisian stations, thermoclines, haloclines and DCM were located relatively deep in the water column, although St17 displayed much more homogeneous profiles (Fig. 8).

T–S diagrams allowed us to identify the main water masses encountered at each station (Fig. 9). At the northern stations (St1–St4) with temperatures of 13.6–14.9 °C and salinities of 37.8–38.4 over 0–150-m depths, we detected (modified) Atlantic Water (AW) coming mainly from the Ligurian Sea and flowing along the continental slope with Ligurian-Provençal current. These "resident" AW (RAW), which have been in the Mediterranean for a long time, have been modified and

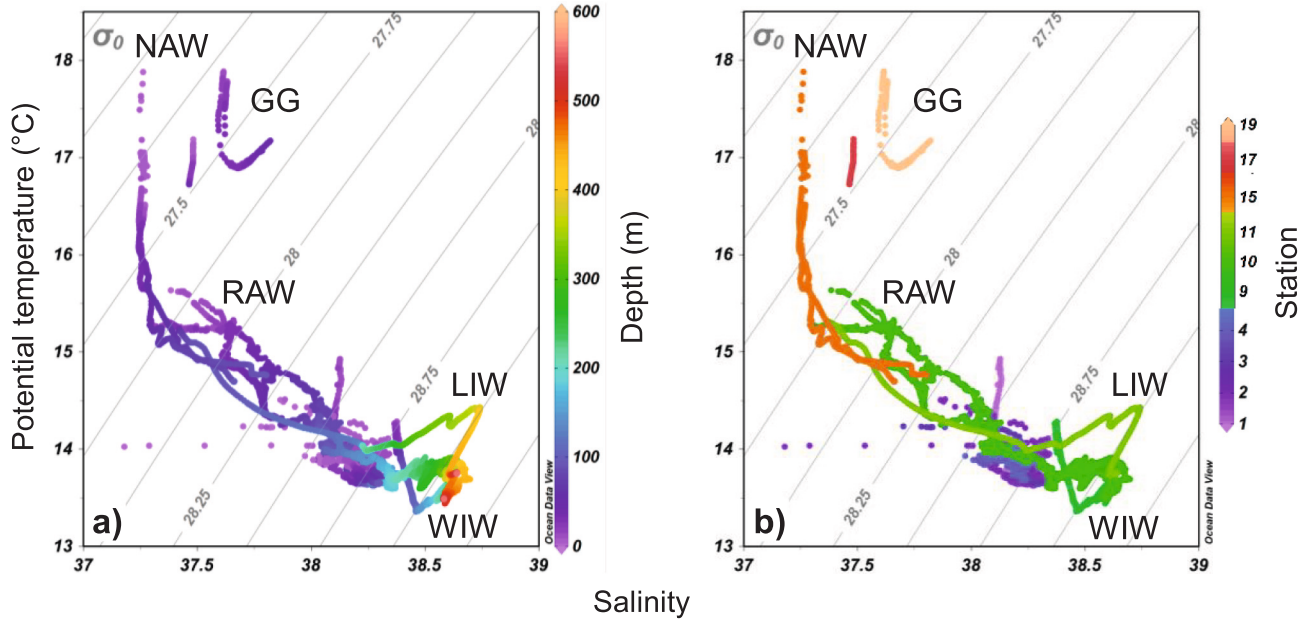

Fig. 9. Temperature-salinity diagram and identification of the main waters masses encountered during the MERITE-HIPPOCAMPE cruise (RAW: resident Atlantic Water; NAW: new Atlantic Water; LIW: Levantine Intermediate Water; WIW: Western Mediterranean Intermediate Water; GG: Gulf of Gabès water). The colour code refers to a) depth (in m) and b) stations (St1–St19). Twenty-one carousel CTD casts were used for this plot. Ocean Data View (ODV) software version 4.6.5. Schlitzer, R., http://odv.awi.de. Schlitzer, 2014.

are saltier (and warmer) than the AW that arrived more recently through the Strait of Gibraltar (Millot and Taupier-Letage, 2005; Balbín et al., 2014). Moving south, St9 was characterised by the presence of RAW over the depth 0–300 m and Levantine Intermediate Water (LIW) over the depth 300–500 m (Fig. 9). LIW is formed in the Eastern Mediterranean Basin by the combined effect of wintertime cooling and summertime evaporation, leading to a warm (temperatures of 13.8–16 °C) and salty (salinities of 38.3–39) intermediate layer that is visible over the whole Mediterranean Sea (Lascaratos et al., 1993; Balbín et al., 2014; Margirier et al., 2020). Once formed, the LIW spreads throughout the entire Eastern and Western Basins and can be identified through a salinity maximum at between ~200 and 600-m depth in the Western Basin before it eventually flows out of the Mediterranean Sea as one of the main components of Mediterranean outflow water (Ben Ismail et al., 2012; Vargaz-Yanez et al., 2012). In addition, the presence of Western Mediterranean Intermediate Water (WIW) was detected at St9 around 100-m depth with temperatures of 13.2–13.9 °C and salinities of 38.4–38.6 (Figs. 7, 9). The WIW forms during winter in the Northwestern Mediterranean Basin due to surface cooling of RAW and intermediate convection (Salat and Font, 1987; Gasparini et al., 1999) and has been recorded in the Algerian Basin by Benzohra and Millot (1995) and in the Sicily Channel by Ben Ismail et al. (2012), flowing eastwards below the AW in the Algerian Current through the Channel of Sardinia. The WIW is characterised by a relative minimum potential temperature located between 100 and 200-m depth. The circulation of WIW has only been investigated in the Algerian Basin, and there is speculation that it follows the same flow paths as the overlying AW (Millot, 1999). St10 and St11 showed weak signature of the WIW and the presence of marked LIW indicating a dominant influence of the northward advection of LIW rather than winter cooling in the water column. The LIW water was well evident in St11, the closest station to the Sardinia Channel (Figs. 8, 9). At the northernmost tip of the Tunisian coast, the water temperature progressively increased and the salinity decreased, revealing the presence of fresher or "new" AW (NAW) coming from the Algerian Basin. The water column arriving at St15, located in the Gulf of Hammamet, was mostly made up of RAW and NAW with temperatures of 14.8–17.5 °C and low salinities of 37.1–37.8 from surface to bottom. Moving southward toward the Gulf of Gabès (GG), the temperature and salinity increased sharply to reach 17.1 °C and 37.5 at St17 and 17.9 °C and 37.8 at St19 (Figs. 8, 9).

3.3. Biogeochemical context

The analytical methods used to determine biogeochemical parameters presented in this section are detailed in Text S1. Considering the whole cruise period, the average (over 32 days) surface TChl*a* concentration derived from satellite data was higher at St9 (~ 1 μg L^{-1}) than in the other stations (< 1 μg L^{-1}) (Fig. 10). The higher content of phytoplankton biomass at St9 was also corroborated in the TChl*a* concentrations actually recorded during the cruise at 5-m depth, either from CTD measurements or analyses on discrete samples (with a significant correlation between both measurements: $r = 0.98$, $n = 10$, $p < 0.0001$; Table S7). In line with the discrete samples, the highest TChl*a* concentrations at 5-m depth were found at St9 (2.90 μg L^{-1}) followed by St4 (1.57 μg L^{-1}) and St1 (0.84 μg L^{-1}), while the lowest TChl*a* concentrations were observed at St17 (0.15 μg L^{-1}) and St15 (0.10 μg L^{-1}) (Table S7).

DCM was shallowest at St4 (13 m), St1 and St9 (20 m) and deepest at St10 (51 m), St2, St3 (53 m) and St15 (66 m) (Figs. 7, 8, 11a; Table S7). TChl*a* in the DCM followed a fairly similar pattern of distribution to TChl*a* at 5-m depth, with a significant correlation between both measures based on both CTD and discrete sample data ($r = 0.64$–0.92, $n = 10$, $p = 0.0001$–0.048). TChl*a* concentrations measured on discrete samples from the DCM were highest at St9 (1.54 μg L^{-1}), in line with the surface/subsurface TChl*a* data (Fig. 10). High TChl*a* concentrations were also recorded south of the Gulf of Gabès (at St19: 1.45 μg L^{-1}) (Fig. 11b; Table S7), even though at this station it was not really a DCM that was observed but rather a bottom-lying bead, as can often be observed for shallow coastal stations. St4 and St1 showed fairly high TChl*a* concentrations of 0.98 and 0.77 μg L^{-1}, respectively. The lowest TChl*a* concentrations in the DCM were found at St17 (0.21 μg L^{-1}), St2, and St11 (0.38 μg L^{-1}) (Fig. 11b; Table S7).

The North-to-South distribution of other biogeochemical parameters measured in the DCM presented interesting features. POC concentration

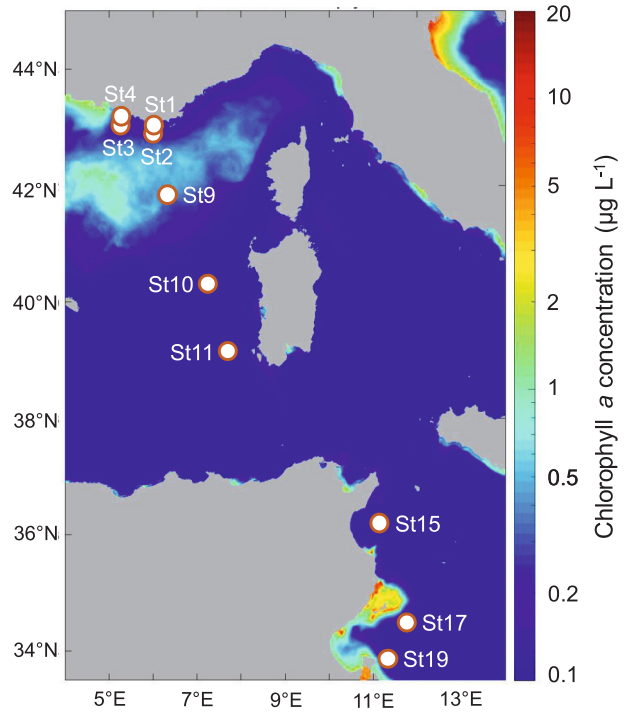

Fig. 10. Composite image of average surface chlorophyll *a* (Chl*a*) concentration (in µg L^{-1}) over the period (13 April–14 May 2019) and area of the MERITE-HIPPOCAMPE cruise from Multi Satellite products (MODIS-AQUA, NOAA20-VIIRS, NPP-VIIRS and Sentinel3A-OLCI) (L4 product level, 1-km resolution; Volpe et al., 2019). This composite image corresponds to the average of the 32 daily images (from 13 April to 14 May 2019) for which Chl*a* concentration was averaged during the 8 h of measurements in the area. Product name: OCEANCOLOUR_MED_CHL_L4_REP_OBSERVATIONS_009_078. Obtained from EU Copernicus Marine Service Information (CMEMS; https://marine.copernicus.eu/). (For interpretation of the references to colour in this figure legend, the reader is referred to the web version of this article.)

had a fairly similar pattern of distribution to TChl*a*, with decreasing values from St1 to St3, a maximal value at St9 (156.4 µg L^{-1}), then a decrease up to St17, and finally a higher value at St19 (55.9 µg L^{-1}) (Fig. 11c; Table S7). $Si(OH)_4$ concentration followed much the same pattern but with an increase from St1 to St3 and a maximal value at both St9 and St19 (~ 2.00 µM) (Fig. 11d; Table S7). NO_3^- concentration increased from St1 to its peak at St3 (1.31 µM), was still high at St9 (0.96 µM), and then decreased along to St17–St19 (Fig. 11e; Table S7). PO_4^{3-} concentration was particularly high at St3 (0.31 µM) and St19 (0.55 µM) (Fig. 11f; Table S7). Finally, DOC concentration and a_{CDOM} decreased from St1 to St9 or St10 then increased up to St19 where they reached maximal values (76.2 µM and 2.05 m^{-1}, respectively) (Fig. 11g, h; Table S7).

Principal component analysis (PCA) based on the Pearson's correlation matrix was applied on these biogeochemical parameters recorded in the DCM at each station (Fig. 12). The first principal component (PC1), which explained 47 % of total variance within samples, was mainly driven by PO_4^{3-}, DOC, a_{CDOM}, and to a lesser extent TChl*a* and $Si(OH)_4$. The second principal component (PC2), which accounted for 34 % of total variance, was driven by POC, NO_3^-, TChl*a*, and $Si(OH)_4$. Four groups of samples (stations) emerged from this PCA: 1) St2, St3, St4, St10, characterised by moderate concentrations of nutrients and TChl*a* and a low organic matter content; 2) St1, St11, St15, St17, with the lowest concentrations in nutrients and TChl*a* (except St1); 3) St9, which showed the highest in $Si(OH)_4$, NO_3^-, TChl*a* and POC concentrations, and the lowest PO_4^{3-} and DOM contents; 4) St19, which showed the highest concentrations in $Si(OH)_4$, TChl*a* (equivalent to those of St9), PO_4^{3-} and DOM as well as high POC and low NO_3^- concentrations (Fig. 12).

Overall, the levels of TChl*a*, nutrients and other biogeochemical parameters observed along the North-South transect in the subsurface waters and DCM in spring 2019 during the MERITE-HIPPOCAMPE cruise are consistent with previous observations in the Mediterranean Sea (The Mermex Group, 2011; Salgado-Hernanz et al., 2019; Guieu et al., 2020; Marañón et al., 2021). The TChl*a* levels in the different stations were also consistent with their positioning in terms of bloom-condition areas and consensus regions defined by D'Ortenzio and d'Alcalà (2009) and Ayata et al. (2018). TChl*a* concentrations tended to be higher at stations located north of the North Balearic front (St1–St4, St9) than stations located south (St10, St11, St15, St17, St19).

Interestingly, two stations, St9 and St19, clearly stood apart from the others in terms of biogeochemical content (Figs. 11, 12). St9 was situated at the boundary of the Ligurian consensus region, in the wintertime deep convection area. Time-series of water temperature recorded at different depths at the LION mooring (42° 02′ N, 4° 40′ E) highlighted a deepening of the mixed layer depth and thus the convection process down to 1500-m depth within the Ligurian area in early February 2019 (Fig. S9). In late March 2019, the end of the convection process induced the occurrence of an intense phytoplankton bloom in the same area (Fig. S9). This illustrates the fact that 2019 was a relatively convective and productive year (Margirier et al., 2020; Bosse et al., 2022), and that St9, located at the border of this convective and productive zone, still presented high concentrations of TChl*a*, POC and some nutrients in the May 2019 sampling period.

The high levels of TChl*a*, $Si(OH)_4$, PO_4^{3-}, DOM, and POC encountered at St19 south of the Gulf of Gabès is probably related to the Saharan dust deposition event (see Section 3.1), but the effect of sediment resuspension cannot be excluded due to high wind speeds during this period (Fig. S8). In the Gulf of Gabès, TChl*a* concentrations can reach >1 µg L^{-1} close to the coast of Djerba and Kerkennah Islands during the spring season (Bel Hassen et al., 2009). The Gulf of Gabès is known to be regularly submitted to Saharan dust deposition (Béjaoui et al., 2019). This Saharan dust, enriched in phosphorus, has been shown to induce phytoplankton blooms in the Gulf (Hamza et al., 2016; Béjaoui et al., 2019), and as described above, intense Saharan dust deposition events occurred in this area during the cruise, for which we collected on-board rain and particle samples (Table 3; Figs. 5; S7, S8). Furthermore, in this shallow ecosystem submitted to strong tides and resulting currents, disturbance and resuspension of sediments could release elements such as nutrients and organic matter into the water column, which in turn may stimulate planktonic activity (Bel Hassen et al., 2009; Fourati et al., 2018; Zouch et al., 2018).

4. Overview of the types of articles produced through the cruise

Fig. 13 shows the types of articles that are a part of this special issue in the frame of the MERITE-HIPPOCAMPE cruise. There are a series of articles concerning the transfer and accumulation of contaminants in planktonic food webs in the DCM but also in surface/subsurface waters. These articles present: 1) contaminant concentrations in the different planktonic/particulate size fractions and, for several of them, in the dissolved phase of water (see Table S6 for the size fractions–contaminant analysis correspondence), and 2) their resulting factors of bioconcentration, bioaccumulation or food accumulation. The contaminants investigated are trace metals/metalloids (Cr, Mn, Fe, Co, Ni, Cu, Zn, As, Se, Mo, Ag, Cd, Sb, Pb…) (Chifflet et al., 2023), with a focus on Cu and Zn isotopes (Chifflet et al., 2022), Hg and MeHg (Tesán Onrubia et al., in prep.), PAHs (Guigue et al., in prep.), PCBs, PBDEs, PFASs (Tronczynski et al., in prep.), and radionuclides (^{137}Cs) (Radakovitch et al., in prep.). Another work will treat of the abundance and composition of microplastics in both surface waters and the DCM (Fig. 13).

There are also a series of articles dealing with the composition and structure of planktonic food webs. Indeed, the paper by Tesán-Onrubia et al. (2023) on the stable C and N isotopes ($\delta^{13}C$, $\delta^{15}N$) and biochemical

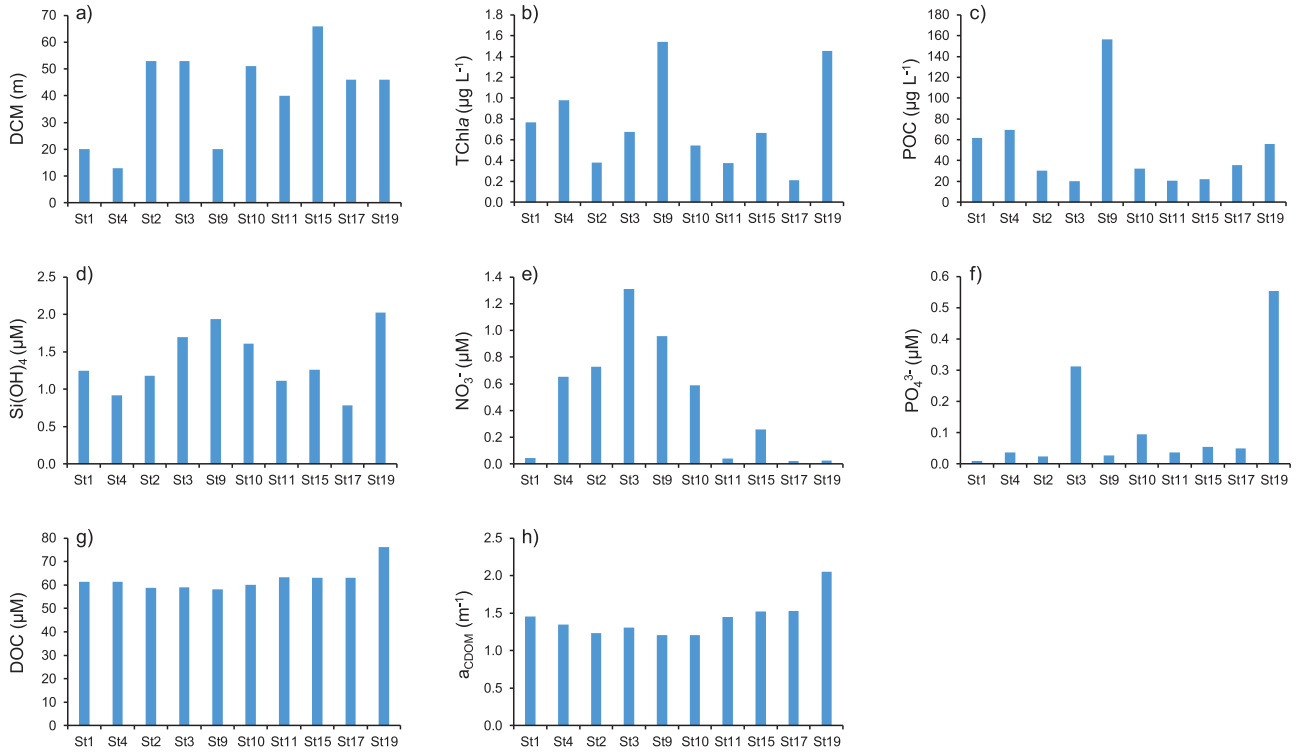

Fig. 11. Distribution of various biogeochemical parameters recorded at the deep chlorophyll maximum (DCM) across the ten stations, from the most coastal stations in the North (St1, St4) to the southernmost stations (St17, St19): a) depth of the DCM (in m), concentrations in b) total chlorophyll *a* (TChl*a*, in µg L^{-1}), c) particulate organic carbon (POC, in µg L^{-1}), d) silicates [$Si(OH)_4$, in µM], e) nitrates (NO_3^-, in µM), f) phosphates (PO_4^{3-}, in µM), g) dissolved organic carbon (DOC, in µM), and h) absorption of chromophoric dissolved organic matter at 254 nm (a_{CDOM}, in m^{-1}). Nutrients, DOC and a_{CDOM} were measured on the fraction <0.7 µm, while TChl*a* and POC were measured on the fraction >0.7 µm from samples collected with Niskin X bottles.

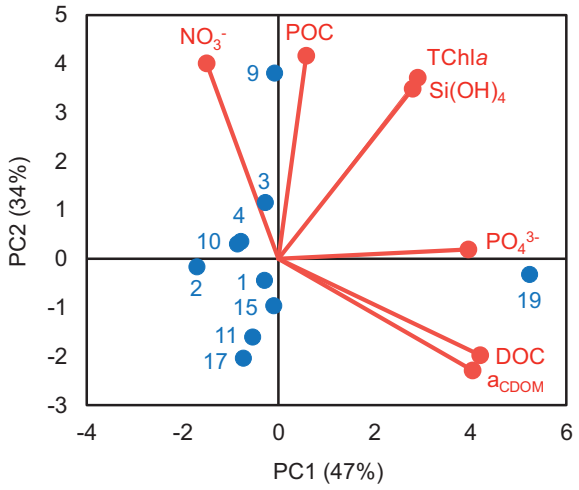

Fig. 12. Principal component analysis (PCA), based on the Pearson's correlation matrix, applied on the main biogeochemical parameters recorded at each stations (St1–19) in the deep chlorophyll maximum (DCM): concentrations in silicates [$Si(OH)_4$, in µM], nitrates (NO_3^-, in µM), phosphates (PO_4^{3-}, in µM), total chlorophyll *a* (TChl*a*, in µg L^{-1}), particulate organic carbon (POC, in µg L^{-1}), dissolved organic carbon (DOC, in µM) and absorption of chromophoric dissolved organic matter at 254 nm (a_{CDOM}, in m^{-1}). Projection of variables (i.e., main biogeochemical parameters, in red) and distribution of samples (i.e., stations, in blue) on the first factorial plane (PC1 versus PC2). Four groups of samples (stations) are highlighted from this PCA and confirmed by a hierarchical ascendant classification (dissimilarity measurement between clusters based on Ward's method): 1) St2, St3, St4, St10, 2) St1, St11, St15, St17, 3) St9, and 4) St19. (For interpretation of the references to colour in this figure legend, the reader is referred to the web version of this article.)

content (lipids, carbohydrates, proteins) of the different planktonic size fractions serves to highlight the structure of planktonic food webs and the transfer of organic matter within them, and to assess the factors of trophic accumulation used in the contaminant-related papers. Moreover, several articles use the cytometry and taxonomy/microscope analyses, imaging (zooscan, flowcam), optical in situ measurements (LOPC, LISST-HOLO) and/or 16S and 18S rRNA high-throughput sequencing analyses to cover the abundance, biomass, distribution, size structure, and composition/diversity of the following planktonic groups, mostly for the DCM but also for surface/subsurface waters or even within the 0–200-m depth layer (see Table S6 for the correspondence with size fractions): pico-, nano- and micro-phytoplankton (Boudriga et al., 2022; Bellaaj Zouari et al., in prep.), micro- and meso-zooplankton and their biomass ratio with detritus (Fierro-González et al., 2023), as well as free-living and plankton-associated bacterioplankton (heterotrophic prokaryotes) (Bellaaj Zouari et al., in prep.; Quéméneur et al., in prep.), and nano- and micro-zooplankton related to the microbial loop (Bellaaj Zouari et al., in prep.). In addition, a complementary paper proposes a methodological approach for the study of the microbiota associated with plankton (Cabrol et al., in prep.). Also, the effect of the Saharan dust deposition event on pico- and nano-phytoplankton community in the south of Gabès is covered by Boudriga et al. (in prep.). Overall, these articles will allow us to understand which planktonic groups are present and how they influence/participate in transfers of contaminants within planktonic networks. Our understanding of the contaminant transfer processes at work within planktonic food webs is also enhanced by the dilution experiments and the subsequent determination of phytoplankton production rates and micro- and meso-zooplankton grazing rates (Meddeb et al., in prep.) (Fig. 13), as well as the grazing and excretion rates estimated from the zooplankton size-structure according to allometric relationships allowing an estimation of grazing pressure and nutrient recycling by the

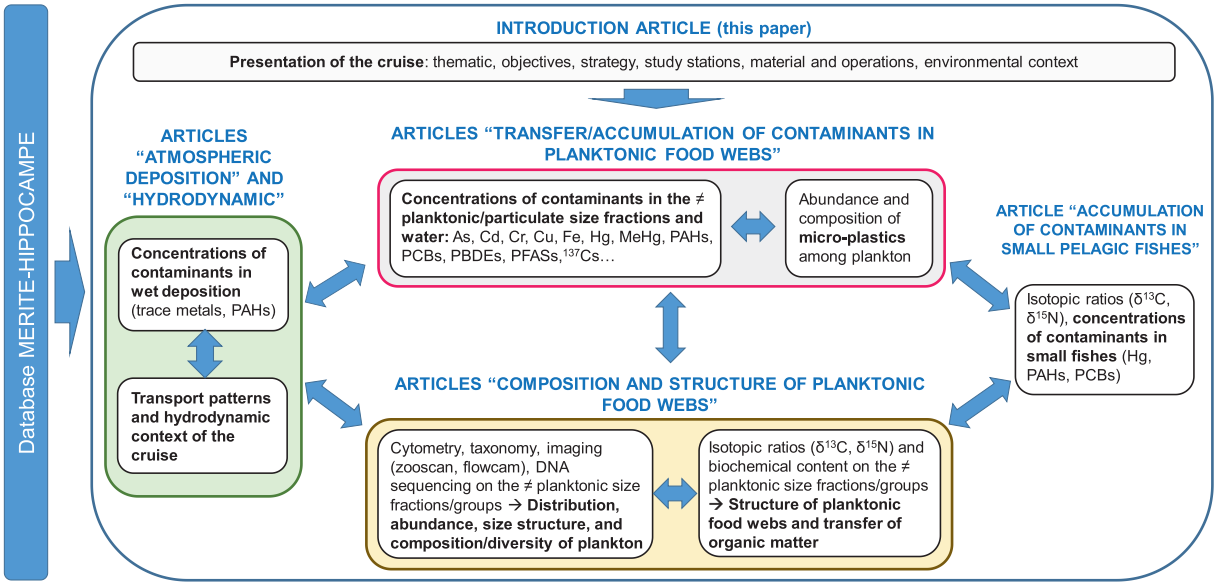

Fig. 13. Overview of the types of articles that are a part of this special issue in the frame of the MERITE-HIPPOCAMPE cruise.

metazooplankton (Fierro-González et al., 2023).

Looking beyond plankton, there is one article dedicated to $\delta^{13}C$ and $\delta^{15}N$ stable isotopes and concentrations of Hg, PAHs and PCBs in small pelagic fishes collected in Tunisian waters (Lajnef et al., in prep.). This study should provide valuable pointers to help establish a link between the contamination of plankton and the contamination of higher trophic levels. The concentrations of trace metals and PAHs in wet (rain) atmospheric deposition samples collected during the cruise and on land is investigated to assess the role of dry/wet atmospheric deposition as a source of contaminants in surface marine waters (Poindron et al., in prep.). Finally, the overall transport patterns and hydrodynamic context of the cruise using modelling and satellite data, and their potential implication for contaminant origin and distribution are addressed by Rwawi et al. (in prep.) (Fig. 13).

CRediT authorship contribution statement

All the authors participated in the MERITE-HIPPOCAMPE project and design of the manuscript.

Conception and design of study: M.T., J.T., F.C., M.P., S.B.I., C.S., M. B.H., K.D., S.C., A.B.Z., D.B., A.B., C.B.-P., N.B., L.C., C.C., L.C., M.N.D. Y., A.D., J.-C.D., C.G., L.G., A.H., L.-E.H.-B., S.J., J.K., B.M., O.P., M.Q., O.R., A.S.H., M.T., N.Z., C.G.

Acquisition of data: M.T., J.T., F.C., M.P., S.B.I., M.B.H., K.D., S.C., A.B.Z., M.A., S.A., L.B.A., N.B., I.B., A.B., N.B., L.C., T. de G.-T., M.F., F. G., L.G., J.K., N.M.B., D.M., J.-C.M., M.M., M.Q., O.R., C.R., A.S.H., J.A. T.O., B.T., M.T., N.Z.

Analysis and/or interpretation of data: M.T., J.T., F.C., M.P., S.B.I., M M.B.H., K.D., C.P., S.C., A.B.Z., S.A., D.B., L.B.A, I.B., A.B., C.B.-P., N. B., L.C., C.C., L.C., S.C., A.D., B.E., P.F.-G., N.G., F.G., C.G., L.G., A.H., L.-E.H.-B., S.J., J.K., R.L., N.M.B, P.L.M., A.B., M.M., B.M., M.Q., O.R., P.R., V.R., C.R., A.S.H., J.A.T.O., B.T., M.T., N.Z.

Drafting the manuscript: M.T., J.T., F.C., M.P., S.B.I., K.D., C.P., S.C., P.L.M., A.B.

Revising/editing the manuscript: J.T., F.C., M.P., C.S., M.B.H., K.D., C.P., A.B.Z., M.A., S.A., D.B., L.B.A., N.B., I.B., A.B., C.B.-P., N.B., L.C., C. C., L.C., S.C., M.N.D.Y., T. de G.-T., A.D., J.-C.D., B.E., P.F.-G., M.F., N. G., F.G., C.G., L.G., A.H., L.-E.H.-B., S.J., J.K., R.L., N.M.B., D.M., A.B., J.-C.M., M.M., B.M., O.P., M.Q., O.R., P.R., C.R., V.R., C.R., A.S.H., J.A.T. O., B.T., M.T., N.Z.

Project administration and funding acquisition: M.T., J.T., F.C., M.P., K.D., C.S.

Declaration of competing interest

The authors declare that they have no known competing financial interests or personal relationships that could have appeared to influence the work reported in this paper.

Data availability

All data from the MERITE-HIPPOCAMPE cruise (https://doi.org/10.17600/18000900; Tedetti and Tronczynski, 2019) is stored in the MISTRALS-SEDOO database (https://mistrals.sedoo.fr/MERITE/) and will be made publicly accessible once all the articles related to the cruise are published in the present special issue. In the meantime, data can be obtained upon request from the corresponding author. In addition, navigation data and CTD profiles from the MERITE-HIPPOCAMPE cruise are available via the IFREMER/SISMER database (https://data.ifremer.fr/SISMER).

Acknowledgments

The MERITE-HIPPOCAMPE project was initiated and funded by the cross-disciplinary *Pollution & Contaminants* axis of the CNRS-INSU MISTRALS program (joint action of the MERMEX-MERITE and CHARMEX subprograms). The project also received financial support from the IRD French-Tunisian International Joint Laboratory (LMI) COSYS-Med. The MERITE-HIPPOCAMPE cruise was organised and supported by the French Oceanographic Fleet (FOF), CNRS/INSU, IFREMER, IRD, the Tunisian Ministry of Agriculture, Water Resources and Fisheries, and the Tunisian Ministry of Higher Education and Scientific Research. The project also benefited from additional funding by IFREMER, by the MIO Action Sud and Transverse Axis programs (CONTAM Transverse Axis), by the IRD Ocean Department, and by the CONTAMPUMP project, funded by the French National Research Agency (ANR) (ANR JCJC #19-CE34-0001-01). It was also supported by the Chemical and Physical Properties of the Atmosphere (CaPPA) project, funded by the ANR through the Programme d'Investissement d'Avenir (PIA) under contract ANR-11-LABX-0005-01, and by the Regional Council Nord-Pas de Calais and the European Funds for Regional Economic Development (FEDER). We are grateful to the captains and crew of the R/V *Antea* for their help and assistance during the cruise, as well as to the captain and crew of the R/V *Hannibal* (INSTM, Tunisia) for sampling small pelagic fishes in the Tunisian waters. We also thank the captain and crew of the R/V *Antédon*

2 for the pre-HIPPOCAMPE cruise performed in the Bay of Marseille in 2018. IFREMER-FOF and Genavir teams provided valuable technical and administrative support for the preparation and conduct of the cruise. We warmly thank P. Vert, F. André and A. Miere from Observatoire Midi-Pyrénées/SEDOO for the implementation of the HIPPOCAMPE Operation Centre (http://hippoc.sedoo.fr/) and the MERITE-HIPPOCAMPE database (https://mistrals.sedoo.fr/MERITE/). We also thank F. Dulac (LSCE) for his contribution in the early phases of the project. We thank E. de Saint-Léger and F. Perault (DT-INSU, Brest) for provisioning the in situ McLane pumps with sequential filtration units, and A. Smirnov (NASA Goddard Space Flight Centre) for provisioning the Microtops sunphotometer. The IRD's representation in Tunisia, the French Institute of Tunisia, and INSTM provided valuable logistics and/or financial assistance to help prepare the cruise, and CNRS-INSU, IFREMER, IRD, IRSN and MIO communications and outreach divisions helped promote the campaign. We are grateful to the Station Marine d'Endoume (OSU Institut Pythéas, Aix-Marseille Université, CNRS) and to the INSTM for providing the facilities to host the atmospheric deposition collectors in Marseille and Sfax. We thank L. Casalot (MIO) and the IRD for helpful support on implementing the "Accès et partage des avantages découlant de l'utilisation des ressources génétiques et des connaissances traditionnelles associées" (APA) procedure. Various MIO platforms also provided valuable support: the Service Atmosphère-Mer (SAM), for preparation and management of the embarked material, the Plateforme Analytique de Chimie des Environnements Marins (PACEM platform) for various chemical analyses, the Platform Microscopie et Imagerie (MIM platform) for plankton analyses, and the Plateforme Régionale de Cytométrie pour la Microbiologie (PRECYM platform) for cytometric analyses. L. Gouriou (IFREMER, LER-AR Arcachon) ran HPLC analyses of the pigments. I. Fronval and V. Riffault (IMT NE) performed the analyses of PAHs in atmospheric deposition and contributed to data interpretation. We used imagery taken from the NASA Worldview application (https://worldview.earthdata.nasa.gov), which is part of the NASA Earth Observing System Data and Information System (EOSDIS). Data and/or images from the NMMB/BSC-Dust or BSC-DREAM8b model were produced by the Barcelona Supercomputing Centre (http://www.bsc.es/ess/bsc-dust-daily-forecast/). The average surface Chl*a* image was obtained from EU Copernicus Marine Service Information (CMEMS; https://marine.copernicus.eu/). This paper and special issue are dedicated to our friend and colleague, Cédric Garnier, who passed away in 2018. Cédric was a deeply-involved and very active member of the MERMEX-MERITE program, and was part of the team that initiated and promoted the MERITE-HIPPOCAMPE cruise project. Finally, we are grateful to two anonymous reviewers for their helpful and constructive comments and corrections.

Appendix A. Supplementary data

Supplementary data to this article can be found online at https://doi.org/10.1016/j.marpolbul.2023.114765.

References

Alcaraz, M., Calbet, A., 2003. Zooplankton ecology. Mar. Ecol. 16.

Alekseenko, E., Thouvenin, B., Tronczyński, J., Carlotti, F., Garreau, P., Tixier, C., Baklouti, M., 2018. Modeling of PCB trophic transfer in the Gulf of Lions; 3D coupled model application. Mar. Pollut. Bull. 128, 140–155. https://doi.org/10.1016/j.marpolbul.2018.01.008.

Ayata, S.D., Irisson, J.O., Aubert, A., Berline, L., Dutay, J.C., Mayot, N., Nieblas, A.E., D'Ortenzio, F., Palmieri, J., Reygondeau, G., Rossi, V., Guieu, C., 2018. Regionalisation of the Mediterranean basin, a MERMEX synthesis. Prog. Oceanogr. 163, 7–20. https://doi.org/10.1016/j.pocean.2017.09.016.

Balbín, R., López-Jurado, J., Flexas, M., Reglero, P., Vélez-Velchí, P., González-Pola, C., Rodríguez, J., García, A., Alemanya, F., 2014. Interannual variability of the early summer circulation around the Balearic Islands: driving factors and potential effects on the marine ecosystem. J. Mar. Syst. 138, 70–81. https://doi.org/10.1016/j.jmarsys.2013.07.004.

Barhoumi, B., Castro-Jiménez, J., Guigue, C., Goutx, M., Sempéré, R., Derouiche, A., Achour, A., Touil, S., Driss, M.R., Tedetti, M., 2018. Levels and risk assessment of hydrocarbons and organochlorines in aerosols from a north African coastal city (Bizerte, Tunisia). Environ. Pollut. 240, 422–431. https://doi.org/10.1016/j.envpol.2018.04.109.

Barral, Q.B., Zakardjian, B., Dumas, F., Garreau, P., Testor, P., Beuvier, J., 2021. Characterization of fronts in the Western Mediterranean with a special focus on the North Balearic Front. Prog. Oceanogr. 197, 102636 https://doi.org/10.1016/j.pocean.2021.102636.

Barrier, N., Petrenko, A.A., Ourmières, Y., 2016. Strong intrusions of the Northern Mediterranean current on the eastern Gulf of Lion: insights from in-situ observations and high resolution numerical modelling. Ocean Dyn. 66, 313–327. https://doi.org/10.1007/s10236-016-0921-7.

Béjaoui, B., Ben Ismail, S., Othmani, A., Othmani Ben Abdallah-Ben Hadj Hamida, O., Chevalier, C., Feki-Sahnoun, W., Harzallah, A., Ben Hadj Hamida, N., Bouaziz, R., Dahech, S., Diaz, F., Tounsi, K., Sammari, C., Pagano, M., Bel Hassen, M., 2019. Synthesis review of the Gulf of Gabes (eastern Mediterranean Sea, Tunisia): morphological, climatic, physical oceanographic, biogeochemical and fisheries features. Estuar. Coast. Shelf Sci. 219, 395–408. https://doi.org/10.1016/j.ecss.2019.01.006.

Bel Hassen, M., Hamza, A., Drira, Z., Zouari, A., Akrout, F., Messaoudi, S., Aleya, L., Ayadi, H., 2009. Phytoplankton-pigment signatures and their relationship to spring summer stratification in the Gulf of Gabes. Estuar. Coast. Shelf Sci. 83, 296–306. https://doi.org/10.1016/j.ecss.2009.04.002.

Ben Ismail, S., Sammari, C., Gasparini, G.P., Béranger, K., Brahim, M., Aleya, L., 2012. Water masses exchanged through the Channel of Sicily: evidence for the presence of new water masses on the Tunisian side of the Channel. Deep Sea Res.Part I 63, 65–81. https://doi.org/10.1016/j.dsr.2011.12.009.

Benzohra, M., Millot, C., 1995. Characteristics and circulation of the surface and intermediate water masses off Algeria. Deep-Sea Res. I 42, 1803–1830. https://doi.org/10.1016/0967-0637(95)00043-6.

Berline, L., Rammou, A., Doglioli, A., Molcard, A., Petrenko, A., 2014. A connectivity based ecoregionalization of the Mediterranean Sea. PLoS ONE 9, e111978. https://doi.org/10.1371/journal.pone.0111978.

Berrojalbiz, N., Dachs, J., Ojeda, M.J., Valle, M.C., Castro-Jimenez, J., Wollgast, J., Ghiani, M., Hanke, G., Zaldivar, J.M., 2011. Biogeochemical and physical controls on concentrations of polycyclic aromatic hydrocarbons in water and plankton of the Mediterranean and Black Seas. Glob. Biogeochem. Cycles 25, GB4003. https://doi.org/10.1029/2010GB003775, 2011.

Bishop, J.K.B., Wood, T.J., 2008. Particulate matter chemistry and dynamics in the twilight zone at VERTIGO ALOHA and K2 sites. Deep Sea Res.I 55, 1684–1706. https://doi.org/10.1016/j.dsr.2008.07.012.

Bishop, J.K.B., Lam, P.J., Wood, T.J., 2012. Getting good particles: accurate sampling of particles by large volume in-situ filtration. Limnol. Oceanogr. Methods 10, 681–710. https://doi.org/10.4319/lom.2012.10.681.

Bodiguel, X., Loizeau, V., Le Guellec, A.-M., Roupsard, F., Philippon, X., Mellon-Duval, C., 2009. Influence of sex, maturity and reproduction on PCB and p, p′DDE concentrations and repartitions in the European hake (Merluccius merluccius, L.) from the Gulf of Lions (N.W. Mediterranean). Sci. Total Environ. 408, 304–311. https://doi.org/10.1016/j.scitotenv.2009.10.004.

Bosse, A., Testor, P., Coppola, L., Bretel, P., Dausse, D., Durrieu de Madron, X., Houpert, L., Labaste, M., Legoff, H., Mortier, L., D'Ortenzio, F., 2022. LION observatory data. SEANOE. https://doi.org/10.17882/44411.

Boudriga, I., Thyssen, M., Zouari, A., Garcia, N., Tedetti, M., Bel Hassen, M., 2022. Ultraphytoplankton community structure in subsurface waters along a North-South Mediterranean transect. Mar. Pollut. Bull. 182, 113977 https://doi.org/10.1016/j.marpolbul.2022.113977.

Calidonna, C.R., Avolio, E., Gullì, D., Ammoscato, I., De Pino, M., Donateo, A., Lo Feudo, T., 2020. Five years of dust episodes at the southern Italy GAW regional coastal Mediterranean observatory: multisensors and modeling analysis. Atmosphere 11, 456. https://doi.org/10.3390/atmos11050456.

Casal, P., González-Gaya, B., Zhang, Y., Reardon, A.J.F., Martin, J.W., Jiménez, B., Dachs, J., 2017. Accumulation of perfluoroalkylated substances in oceanic plankton. Environ. Sci. Technol. 51, 2766–2775. https://doi.org/10.1021/acs.est.6b05821.

Castro-Jiménez, J., Berrojalbiz, N., Wollgast, J., Dachs, J., 2012. Polycyclic aromatic hydrocarbons (PAHs) in the Mediterranean Sea: atmospheric occurrence, deposition and decoupling with settling fluxes in the water column. Environ. Pollut. 166, 40–47. https://doi.org/10.1016/j.envpol.2012.03.003.

Castro-Jiménez, J., Barhoumi, B., Paluselli, A., Tedetti, M., Jiménez, B., Muñoz-Arnanz, J., Wortham, H., Driss, M.R., Sempéré, R., 2017. Occurrence, loading and exposure of atmospheric particle-bound POPs at the African and European edges of the western Mediterranean Sea. Environ. Sci. Technol. 51, 13180–13189. https://doi.org/10.1021/acs.est.7b04614.

Castro-Jiménez, J., Bănaru, D., Chen, C.-T., Jiménez, B., Muñoz-Arnanz, J., Deviller, G., Sempéré, R., 2021. Persistent organic pollutants burden, trophic magnification and risk in a pelagic food web from coastal NW Mediterranean Sea. Environ. Sci. Technol. 55, 9557–9568. https://doi.org/10.1021/acs.est.1c00904.

Chifflet, S., Briant, N., Freydier, R., Araújo, D.F., Quéméneur, M., Zouch, H., Bellaaj-Zouari, A., Carlotti, F., Tedetti, M., 2022. Isotopic compositions of copper and zinc in plankton from the Mediterranean Sea (MERITE-HIPPOCAMPE campaign): tracing trophic transfer and geogenic inputs. Mar. Pollut. Bull. 185, 114315 https://doi.org/10.1016/j.marpolbul.2022.114315.

Chifflet, S., Briant, N., Tesán-Onrubia, J.A., Zaaboub, N., Amri, S., Radakovitch, O., Bănaru, D., Tedetti, M., 2023. Distribution and accumulation of metals and metalloids in planktonic food webs of the Mediterranean Sea (MERITE-HIPPOCAMPE campaign). Mar. Pollut. Bull. 186, 114384 https://doi.org/10.1016/j.marpolbul.2022.114384.

Chouvelon, T., Cresson, P., Bouchoucha, M., Brach-Papa, C., Bustamante, P., Crochet, S., Marco-Miralles, F., Thomas, B., Knoery, J., 2018. Oligotrophy as a major driver of

mercury bioaccumulation in medium-to high-trophic level consumers: a marine ecosystem-comparative study. Environ. Pollut. 233, 844–854. https://doi.org/10.1016/j.envpol.2017.11.015.

Chouvelon, T., Strady, E., Harmelin-Vivien, M., Radakovitch, O., Brach-Papa, C., Crochet, S., Knoery, J., Rozuel, E., Thomas, B., Tronczynski, J., Chiffoleau, J.F., 2019. Patterns of trace metal bioaccumulation and trophic transfer in a phytoplankton-zooplankton-small pelagic fish marine food web. Mar. Pollut. Bull. 146, 1013–1030. https://doi.org/10.1016/j.marpolbul.2019.07.047.

Cossa, D., Coquery, M., 2005. The Mediterranean mercury anomaly, a geochemical or a biological issue. In: Saliot, A. (Ed.), The Mediterranean Sea. Handbook of Environmental Chemistry, pp. 177–208.

Cossa, D., Knoery, J., Bănaru, D., Harmelin-Vivien, M., Sonke, J.E., Hedgecock, I.M., Bravo, A.G., Rosati, G., Canu, D., Horvat, M., Sprovieri, F., Pirrone, N., Heimbürger-Boavida, L.E., 2022. Mediterranean mercury assessment 2022: an updated budget, health consequences, and research perspectives. Environ. Sci. Technol. 56, 3840–3862. https://doi.org/10.1021/acs.est.1c03044.

Dachs, J., Méjanelle, L., 2010. Organic pollutants in coastal waters, sediments, and biota: a relevant driver for ecosystems during the Anthropocene? Estuar. Coasts 33, 1–14. https://doi.org/10.1007/s12237-009-9255-8.

Dachs, J., Lohmann, R., Ockenden, W.A., Mejanelle, L., Eisenreich, S.J., Jones, K.C., 2002. Oceanic biogeochemical controls on global dynamics of persistent organic pollutants. Environ. Sci. Technol. 36, 4229–4237. https://doi.org/10.1021/es025724k.

Desboeufs, K., Fu, F., Bressac, M., Tovar-Sánchez, A., Triquet, S., Doussin, J.-F., Giorio, C., Chazette, P., Disnaquet, J., Feron, A., Formenti, P., Maisonneuve, F., Rodríguez-Romero, A., Zapf, P., Dulac, F., Guieu, C., 2022. Wet deposition in the remote western and central Mediterranean as a source of trace metals to surface seawater. Atmos. Chem. Phys. 22, 2309–2332. https://doi.org/10.5194/acp-22-2309-2022.

Ding, Q., Gong, X., Jin, M., Yao, X., Zhang, L., Zhao, Z., 2021. The biological pump effects of phytoplankton on the occurrence and benthic bioaccumulation of hydrophobic organic contaminants (HOCs) in a hypereutrophic lake. Ecotoxicol. Environ. Saf. 213, 112017 https://doi.org/10.1016/j.ecoenv.2021.112017.

D'Ortenzio, F., d'Alcalà, M.R., 2009. On the trophic regimes of the Mediterranean Sea: a satellite analysis. Biogeosciences 6, 139–148. https://doi.org/10.5194/bg-6-139-2009.

Duran, R., Cravo-Laureau, C., 2016. Role of environmental factors and microorganisms in determining the fate of polycyclic aromatic hydrocarbons in the marine environment. FEMS Microbiol. Rev. 40, 814–830. https://doi.org/10.1093/femsre/fuw031.

El Hourany, R., Abboud-Abi Saab, M., Faour, G., Mejia, C., Crépon, M., Thiria, S., 2019. Phytoplankton diversity in the Mediterranean Sea from satellite data using self-organizing maps. J. Geophys. Res. Oceans 124, 5827–5843. https://doi.org/10.1029/2019JC015131.

Elbaz-Poulichet, F., Morley, N.H., Beckers, J.-M., Nomerange, P., 2001. Metal fluxes through the Strait of Gibraltar: the influence of the Tinto and Odiel rivers (SW Spain). Mar. Chem. 73, 93–213. https://doi.org/10.1016/S0304-4203(00)00106-7.

Everaert, G., De Laender, F., Goethals, P.L.M., Janssen, C.R., 2015. Multidecadal field data support intimate links between phytoplankton dynamics and PCB concentrations in marine sediments and biota. Environ.Sci.Technol. 49, 8704–8711. https://doi.org/10.1021/acs.est.5b01159.

Fan, C.-W., Reinfelder, J.R., 2003. Phenanthrene accumulation kinetics in marine diatoms. Environ. Sci. Technol. 37, 3405–3412. https://doi.org/10.1021/es026367g.

Fierro-González, P., Pagano, M., Guilloux, L., Makhlouf Belkahia, N., Tedetti, M., Carlotti, F., 2023. Zooplankton Biomass, Size Structure, and Associated Metabolic Fluxes With Focus on Its Roles at the Chlorophyll Maximum Layer During the Plankton-contaminant MERITE-HIPPOCAMPE Cruise. Submitted to this special issue.

Fourati, R., Tedetti, M., Guigue, C., Goutx, M., Garcia, N., Zaghden, H., Sayadi, S., Elleuch, B., 2018. Sources and spatial distribution of dissolved aliphatic and polycyclic aromatic hydrocarbons in surface coastal waters from the Gulf of Gabès (Tunisia, Southern Mediterranean Sea). Prog. Oceanogr. 163, 232–247. https://doi.org/10.1016/j.pocean.2017.02.001.

Frouin, H., Dangerfield, N., Macdonald, R.W., Galbraith, M., Crewe, N., Shaw, P., Mackas, D., Ross, P.S., 2013. Partitioning and bioaccumulation of PCBs and PBDEs in marine plankton from the Strait of Georgia, British Columbia, Canada. Prog. Oceanogr. 115, 65–75. https://doi.org/10.1016/j.pocean.2013.05.023.

Galbán-Malagón, C., Berrojalbiz, N., Ojeda, M.J., Dachs, J., 2012. The oceanic biological pump modulates the atmospheric transport of persistent organic pollutants to the Arctic. Nat. Commun. 3, 862. https://doi.org/10.1038/ncomms1858.

Gasparini, G.P., Zodiatis, G., Astraldi, M., Galli, C., Sparnocchia, S., 1999. Winter intermediate water lenses in the Ligurian Sea. J. Mar. Syst. 20, 319–332. https://doi.org/10.1016/s0924-7963(98)00089-x.

Gonzalez, L., Briottet, X., 2017. North Africa and Saudi Arabia day/night sandstorm survey (NASCube). Remote Sens. 9, 896. https://doi.org/10.3390/rs9090896.

González-Gaya, B., Martínez-Varela, A., Vila-Costa, M., Casal, P., Cerro-Gálvez, E., Berrojalbiz, N., Lundin, D., Vidal, M., Mompean, C., Bode, A., Jiménez, B., Dachs, J., 2019. Biodegradation as an important sink of aromatic hydrocarbons in the oceans. Nat.Geosci. 12, 119–125. https://doi.org/10.1038/s41561-018-0285-3.

Guieu, C., D'Ortenzio, F., Dulac, F., Taillandier, V., Doglioli, A., Petrenko, A., Barrillon, S., Mallet, M., Nabat, P., Desboeufs, K., 2020. Introduction: process studies at the air–sea interface after atmospheric deposition in the Mediterranean Sea – objectives and strategy of the PEACETIME oceanographic campaign (May–June 2017). Biogeosciences 17, 5563–5585. https://doi.org/10.5194/bg-17-5563-2020, 2020.

Guigue, C., Tedetti, M., Ferretto, N., Garcia, N., Méjanelle, L., Goutx, M., 2014. Spatial and seasonal variabilities of dissolved hydrocarbons in surface waters from the Northwestern Mediterranean Sea: results from one year intensive sampling. Sci. Total Environ. 466–467, 650–662. https://doi.org/10.1016/j.scitotenv.2013.07.082.

Hamza, I., Feki, W., Hamza, A., Bel Hassen, M., 2016. Long term characterization of Trichodesmium erythraeum blooms in Gabes Gulf (Tunisia). Cont. Shelf Res. 124, 95–103. https://doi.org/10.1016/j.csr.2016.05.007.

Harmelin-Vivien, M., Cossa, D., Crochet, S., Bănaru, D., Letourneur, Y., Mellon-Duval, C., 2009. Difference of mercury bioaccumulation in red mullets from the north-western Mediterranean and Black seas. Mar. Pollut. Bull. 58, 679–685. https://doi.org/10.1016/j.marpolbul.2009.01.004.

Heimbürger, L.E., Cossa, D., Marty, J.C., Migon, C., Averty, B., Dufour, A., Ras, J., 2010. Methylmercury distributions in relation to the presence of nano and picophytoplankton in an oceanic water column (Ligurian Sea, North-western Mediterranean). Geochim.Cosmochim.Acta 74, 5549–5559. https://doi.org/10.1016/j.gca.2010.06.036.

Heimbürger, L.E., Migon, C., Cossa, D., 2011. Impact of atmospheric deposition of anthropogenic and natural trace metals on Northwestern Mediterranean surface waters: a box model assessment. Environ. Pollut. 159, 1629–1634. https://doi.org/10.1016/j.envpol.2011.02.046.

Hinrichsen, D., 1990. Our Common Seas: Coasts in Crisis. Earthscan Publications, London, in association with United Nations Environment Programme, Nairobi, 184 pp.

Hunt, B.P.V., Carlotti, F., Donoso, K., Pagano, M., D'Ortenzio, F., Taillandier, V., Conan, P., 2017. Trophic pathways of phytoplankton size classes through the zooplankton food web over the spring transition period in the north-west Mediterranean Sea. J. Geophys. Res. Oceans 122, 6309–6324. https://doi.org/10.1002/2016JC012658.

Jacquet, S., Monnin, C., Herlory, O., Mille, D., Dufour, A., Oursel, B., Heimbürger-Boavida, L.E., D'onofrio, S., Layglon, N., Garnier, C., 2021. Characterization of the submarine disposal of a Bayer effluent (Gardanne alumina plant, southern France): I. Size distribution, chemical composition and settling rate of particles forming at the outfall. Chemosphere 263, 127695. https://doi.org/10.1016/j.chemosphere.2020.127695.

Jiskra, M., Heimbürger-Boavida, L.E., Desgranges, M.M., Petrova, M.V., Dufour, A., Ferreira-Araujo, B., Masbou, J., Chmeleff, J., Thyssen, M., Point, D., Sonke, J.E., 2021. Mercury stable isotopes constrain atmospheric sources to the ocean. Nature 597, 678–682. https://doi.org/10.1038/s41586-021-03859-8.

Jordi, A., Basterretxea, G., Tovar-Sanchez, A., Alastuey, A., Querol, X., 2012. Copper aerosols inhibit phytoplankton growth in the Mediterranean Sea. Proc. Natl. Acad. Sci. 109, 21246–21249. https://doi.org/10.1073/pnas.1207567110.

Köck-Schulmeyer, M., Ginebreda, A., Petrovic, M., Giulivo, M., Aznar-Alemany, Ò., Eljarrat, E., Valle-Sistac, J., Molins-Delgado, D., Diaz-Cruz, M.S., Monllor-Alcaraz, L. S., Guillem-Argiles, N., Martínez, E., Miren, L.A., Llorca, M., Farré, M., Peña, J.M., Mandaric, L., Pérez, S., Majone, B., Bellin, A., Kalogianni, E., Skoulikidis, N.T., Milačič, R., Barceló, D., 2021. Priority and emerging organic microcontaminants in three Mediterranean river basins: occurrence, spatial distribution, and identification of river basin specific pollutants. Sci. Total Environ. 754, 142344 https://doi.org/10.1016/j.scitotenv.2020.142344.

Lascaratos, A., Williams, R.G., Tragou, E., 1993. A mixed-layer study of the formation of levantine intermediate water. J. Geophys. Res. Oceans 98 (C8), 14739–14749.

Leblanc, K., Quéguiner, B., Diaz, F., Cornet, V., Michel-Rodriguez, M., Durrieu de Madron, X., Bowler, C., Malviya, S., Thyssen, M., Gregori, G., Rembauville, M., Grosso, O., Poulain, J., de Vargas, C., Pujo-Pay, M., Conan, P., 2018. Nanoplanktonic diatoms are globally overlooked but play a role in spring blooms and carbon export. Nat.Commun. 9, 953. https://doi.org/10.1038/s41467-018-03376-9.

Lee, C.S., Fisher, N.S., 2016. Methylmercury uptake by diverse marine phytoplankton. Limnol. Oceanogr. 61, 1626–1639. https://doi.org/10.1002/lno.10318.

Lejeusne, C., Chevaldonné, P., Pergent-Martini, C., Boudouresque, C.F., Pérez, T., 2010. Climate change effects on a miniature ocean: the highly diverse, highly impacted Mediterranean Sea. Trends Ecol.Evol. 25, 250–260. https://doi.org/10.1016/j.tree.2009.10.009.

Li, H., Duan, D., Beckingham, B., Yang, Y., Ran, Y., Grathwohl, P., 2020. Impact of trophic levels on partitioning and bioaccumulation of polycyclic aromatic hydrocarbons in particulate organic matter and plankton. Mar. Pollut. Bull. 160, 111527 https://doi.org/10.1016/j.marpolbul.2020.111527.

Li, Z., Chi, J., Wu, Z., Zhang, Y., Liu, Y., Huang, L., Lu, Y., Uddin, M., Zhang, W., Wand, X., Lin, Y., Tong, Y., 2021. Characteristics of plankton hg bioaccumulations based on a global data set and the implications for aquatic systems with aggravating nutrient imbalance. Front.Environ.Sci.Eng. 16, 37. https://doi.org/10.1007/s11783-021-1471-x.

Lipiatou, E., Albaigés, J., 1994. Atmospheric deposition of hydrophobic organic chemicals in the northwestern Mediterranean Sea: comparison with the Rhone river input. Mar. Chem. 46, 153–164. https://doi.org/10.1016/0304-4203(94)90052-3.

Llamas-Dios, M.I., Vadillo, I., Jimenez-Gavilan, P., Candela, L., Corada-Fernandez, C., 2021. Assessment of a wide array of contaminants of emerging concern in a Mediterranean water basin (Guadalhorce river, Spain): motivations for an improvement of water management and pollutants surveillance. Sci. Total Environ. 788, 147822 https://doi.org/10.1016/j.scitotenv.2021.147822.

Marañón, E., Wambeke, F., Uitz, J., Boss, E., Dimier, C., Dinasquet, J., Engel, A., Haëntjens, N., Pérez-Lorenzo, M., Taillandier, V., Zäncker, B., 2021. Deep maxima of phytoplankton biomass, primary production and bacterial production in the Mediterranean Sea. Biogeosciences 18, 1749–1767. https://doi.org/10.5194/bg-18-1749-2021.

Margirier, F., Testor, P., Heslop, E., Mallil, K., Bosse, A., Houpert, L., Mortier, L., Bouin, M.-N., Coppola, L., D'Ortenzio, F., Durrieu de Madron, X., Mourre, B., Prieur, L., Raimbault, P., Taillandier, V., 2020. Abrupt warming and salinification of intermediate waters interplays with decline of deep convection in the Northwestern Mediterranean Sea. Sci. Rep. 10, 20923. https://doi.org/10.1038/s41598-020-77859-5.

Martin, J.H., Knauer, G.A., 1973. The elemental composition of plankton. Geochim. Cosmochim.Acta 37, 1639–1653. https://doi.org/10.1016/0016-7037(73)90154-3.

Mayot, N., D'Ortenzio, F., Uitz, J., Gentili, B., Ras, J., Vellucci, V., Golbol, M., Antoine, D., Claustre, H., 2017. Influence of the phytoplankton community structure on the spring and annual primary production in the northwestern Mediterranean Sea. J. Geophys. Res. Oceans 122, 9918–9936. https://doi.org/10.1002/2016JC012668.

Millot, C., 1999. Circulation in the Western Mediterranean Sea. J. Mar. Syst. 20, 423–442. https://doi.org/10.1016/S0924-7963(98)00078-5.

Millot, C., Taupier-Letage, I., 2005. Circulation in the Mediterranean Sea. In: The Handbook of Environmental Chemistry, vol. K 29–66. https://doi.org/10.1007/b107143.

Morales, L., Dachs, J., Fernández-Pinos, M.C., Berrojalbiz, N., Mompean, C., González-Gaya, B., Jiménez, B., Bode, A., Abalos, M., Abad, E., 2015. Oceanic sink and biogeochemical controls on the accumulation of polychlorinated dibenzo-pdioxins, dibenzofurans, and biphenyls in plankton. Environ. Sci. Technol. 49, 13853–13861. https://doi.org/10.1021/acs.est.5b01360.

Nizzetto, L., Gioia, R., Li, J., Borga, K., Pomati, F., Bettinetti, R., Dachs, J., Jones, K.C., 2012. Biological pump control of the fate and distribution of hydrophobic organic pollutants in water and plankton. Environ. Sci. Technol. 46, 3204–3211. https://doi.org/10.1021/es204176q.

Oursel, B., Garnier, C., Durrieu, G., Mounier, S., Omanović, D., Lucas, Y., 2013. Dynamics and fates of trace metals chronically input in a Mediterranean coastal zone impacted by a large urban area. Mar. Pollut. Bull. 69, 137–149. https://doi.org/10.1016/j.marpolbul.2013.01.023.

Radakovitch, O., Roussiez, V., Ollivier, P., Ludwig, W., Grenz, C., Probst, J.L., 2008. Particulate heavy metals input from rivers and associated sedimentary deposits on the Gulf of Lion continental shelf. Estuar. Coast. Shelf Sci. 77, 285–295. https://doi.org/10.1016/j.ecss.2007.09.028.

Ramírez-Romero, E., Molinero, J.C., Sommer, U., Salhi, N., Kefi-Daly Yahia, O., Daly Yahia, M.N., 2020. Phytoplankton size changes and diversity loss in the southwestern Mediterranean Sea in relation to long-term hydrographic variability. Estuar. Coast. Shelf Sci. 235, 106574 https://doi.org/10.1016/j.ecss.2019.106574.

Reygondeau, G., Irisson, J.-O., Ayata, S., Gasparini, S., Benedetti, F., Albouy, C., Hattab, T., Guieu, C., Koubbi, P., 2014. Definition of the Mediterranean Eco-Regions and Maps of Potential Pressures in These Eco-Regions. Technical Report. Deliverable Nr. 1.6. FP7-PERSEUS Project.

Reygondeau, G., Guieu, C., Benedetti, F., Irisson, J.O., Ayata, S.D., Gasparini, S., Koubbi, P., 2017. Biogeochemical regions of the Mediterranean Sea: an objective multidimensional and multivariate environmental approach. Prog. Oceanogr. 151, 138–148. https://doi.org/10.1016/j.pocean.2016.11.001.

Salat, J., Font, J., 1987. Water mass structure near and off shore the Catalan coast during the winters of 1982 and 1983. Ann. Geophys. 1B, 49–54.

Salgado-Hernanz, P.M., Racault, M.-F., Font-Muñoz, J.S., Basterretxea, G., 2019. Trends in phytoplankton phenology in the Mediterranean Sea based on ocean-colour remote sensing. Remote Sens. Environ. 221, 50–64. https://doi.org/10.1016/j.rse.2018.10.036.

Salhi, N., Zmerli Triki, H., Molinero, J.C., Laabir, M., Sehli, E., Bellaaj-Zouari, A., Daly Yahia, N., Kefi-Daly Yahia, O., 2018. Seasonal variability of picophytoplankton under contrasting environments in northern Tunisian coasts, southwestern Mediterranean Sea. Mar. Pollut. Bull. 129, 866–874. https://doi.org/10.1016/j.marpolbul.2017.10.029.

Schlitzer, R., 2014. Ocean Data View. http://odv.awi.de. Available online at.

Ser-Giacomi, E., Jordá-Sánchez, G., Sotto-Navarro, J., Thomsen, S., Mignot, J., Sevault, F., Rossi, V., 2020. Impact of climate change on surface stirring and transport in the Mediterranean Sea. Geophys. Res. Lett. 47, e2020GL089941 https://doi.org/10.1029/2020GL089941.

Sicre, M.-A., Fernandes, M.B., Pont, D., 2008. Poly-aromatic hydrocarbon (PAH) inputs from the Rhône River to the Mediterranean Sea in relation with the hydrological cycle: impact of floods. Mar. Pollut. Bull. 56, 1935–1942. https://doi.org/10.1016/j.marpolbul.2008.07.015.

Siokou-Frangou, I., Christaki, U., Mazzocchi, M.G., Montresor, M., Ribera D'Alcala, M., Vaque, D., Zingone, A., 2010. Plankton in the open mediterranean sea: a review. Biogeosciences 7, 1543–1586. https://doi.org/10.5194/bg-7-1543-2010.

Strady, E., Harmelin-Vivien, M., Chiffoleau, J.F., Veron, A., Tronczynski, J., Radakovitch, O., 2015. 210Po and 210Pb trophic transfer within the phytoplankton–zooplankton–anchovy/sardine food web: a case study from the Gulf of Lion (NW Mediterranean Sea. J. Environ. Radioact. 143, 141–151. https://doi.org/10.1016/j.jenvrad.2015.02.019.

Swackhamer, D.L., Skoglund, R.S., 1993. Bioaccumulation of PCBs by algae: kinetics versus equilibrium. Environ. Toxicol. Chem. 12, 831–838. https://doi.org/10.1002/etc.5620120506.

Tang, J., Wang, S., Tai, Y., Tam, N.F., Su, L., Shi, Y., Luo, B., Tao, R., Yang, Y., Zhang, X., 2020. Evaluation of factors influencing annual occurrence, bioaccumulation, and biomagnification of antibiotics in planktonic food webs of a large subtropical river in South China. Water Res. 170, 115302 https://doi.org/10.1016/j.watres.2019.115302.

Tao, Y., Xue, B., Lei, G., Liu, F., Wang, Z., 2017a. Effects of climate change on bioaccumulation and biomagnification of polycyclic aromatic hydrocarbons in the planktonic food web of a subtropical shallow eutrophic lake in China. Environ. Pollut. 223, 624–634. https://doi.org/10.1016/j.envpol.2017.01.068.

Tao, Y., Yu, J., Xue, B., Yao, S., Wang, S., 2017b. Precipitation and temperature drive seasonal variation in bioaccumulation of polycyclic aromatic hydrocarbons in the planktonic food webs of a subtropical shallow eutrophic lake in China. Sci. Total Environ. 583, 447–457. https://doi.org/10.1016/j.scitotenv.2017.01.100.

Tao, Y., Yu, J., Liu, X., Xue, B., Wang, S., 2018. Factors affecting annual occurrence, bioaccumulation, and biomagnification of polycyclic aromatic hydrocarbons in plankton food webs of subtropical eutrophic lakes. Water Res. 132, 1–11. https://doi.org/10.1016/j.watres.2017.12.053.

Tedetti, M., Tronczynski, J., 2019. HIPPOCAMPE Cruise. RV Antea. https://doi.org/10.17600/18000900.

Tedetti, M., Guigue, C., Goutx, M., 2010. Utilization of a submersible UV fluorometer for monitoring anthropogenic inputs in the Mediterranean coastal waters. Mar. Pollut. Bull. 60, 350–362. https://doi.org/10.1016/j.marpolbul.2009.10.018.

Tesán-Onrubia, J.A., Tedetti, M., Carlotti, F., Tenaille, M., Guilloux, L., Pagano, M., Lebreton, B., Guillou, G., Fierro-González, P., Guigue, C., Chifflet, S., Garcia, T., Boudriga, I., Belhassen, M., Bellaaj-Zouari, M., Banaru, D., 2023. Spatial variations of biochemical content and stable isotope ratios of size-fractionated plankton in the Mediterranean Sea (MERITE-HIPPOCAMPE campaign). Mar. Pollut. Bull. 189, 114787. https://doi.org/10.1016/j.marpolbul.2023.114787.

The MerMex Group, 2011. Marine ecosystems'responses to climatic and anthropogenic forcings in the Mediterranean. Prog. Oceanogr. 91, 97–166. https://doi.org/10.1016/j.pocean.2011.02.003.

Thieuleux, F., Moulin, C., Bréon, F.M., Maignan, F., Poitou, J., Tanré, D., 2005. Remote sensing of aerosols over the oceans using MSG/SEVIRI imagery. Ann. Geophys. 23, 3561–3568. https://doi.org/10.5194/angeo-23-3561-2005.

Thomas, D.M., Lee, C.-S., Fisher, N.S., 2018. Bioaccumulation and trophic transfer of 137Cs in marine and freshwater plankton. Chemosphere 209, 599–607. https://doi.org/10.1016/j.chemosphere.2018.06.124.

Tiano, M., Tronczyński, J., Harmelin-Vivien, M., Tixier, C., Carlotti, F., 2014. PCB concentrations in plankton size classes, a temporal study in Marseille Bay, Western Mediterranean Sea. Mar. Pollut. Bull. 89, 331–339. https://doi.org/10.1016/j.marpolbul.2014.09.040.

Tornero, V., Hanke, G., 2016. Chemical contaminants entering the marine environment from sea-based sources: a review with a focus on European seas. Mar. Pollut. Bull. 112, 17–38. https://doi.org/10.1016/j.marpolbul.2016.06.091.

Uitz, J., Claustre, H., Morel, A., Hooker, S.B., 2006. Vertical distribution of phytoplankton communities in open ocean: an assessment based on surface chlorophyll. J. Geophys. Res. Oceans 111, C08005. https://doi.org/10.1029/2005JC003207.

UNEP/MAP, 2012. State of the Mediterranean Marine and Coastal Environment. UNEP/MAP – Barcelona Convention, Athens.

Vargaz-Yanez, M., Mallard, E.R.M., Zunino, P., Garcia-Martinez, M., Moya, F., 2012. The effect of interpolation methods in temperature and salinity trends in the western Mediterranean. Mediterr. Mar. Sci. 13, 118–125. https://doi.org/10.12681/mms.28.

Volpe, G., Colella, S., Brando, V.E., Forneris, V., La Padula, F., Di Cicco, A., Sammartino, M., Bracaglia, M., Artuso, F., Santoleri, R., 2019. Mediterranean ocean colour Level 3 operational multi-sensor processing. Ocean Sci. 15, 127–146. https://doi.org/10.5194/os-15-127-2019.

Zouch, H., Cabrol, L., Chifflet, S., Tedetti, M., Karray, F., Zaghden, H., Sayadi, S., Quéméneur, M., 2018. Effect of acidic industrial effluent release on microbial diversity and trace metal dynamics during resuspension of coastal sediment. Front. Microbiol. 9, 3103. https://doi.org/10.3389/fmicb.2018.03103.